

## 1 Title

2 **Multioomic Body Mass Index signatures in blood reveal clinically relevant population**  
3 **heterogeneity and variable responses to a healthy lifestyle intervention**  
4

## 5 Authors

6 Kengo Watanabe<sup>1</sup>, Tomasz Wilmanski<sup>1</sup>, Christian Diener<sup>1</sup>, John C. Earls<sup>1,2</sup>, Anat Zimmer<sup>1,†</sup>, Briana  
7 Lincoln<sup>1</sup>, Jennifer J. Hadlock<sup>1</sup>, Jennifer C. Lovejoy<sup>1</sup>, Sean M. Gibbons<sup>1,3,4</sup>, Andrew T. Magis<sup>1</sup>, Leroy  
8 Hood<sup>1,5</sup>, Nathan D. Price<sup>1,2</sup>, and Noa Rappaport<sup>1,\*</sup>  
9

## 10 Affiliations

11 <sup>1</sup>Institute for Systems Biology, Seattle, WA 98109, USA.

12 <sup>2</sup>Thorne HealthTech, New York, NY 10019, USA.

13 <sup>3</sup>Department of Bioengineering, University of Washington, Seattle, WA 98195, USA.

14 <sup>4</sup>eScience Institute, University of Washington, Seattle, WA 98195, USA.

15 <sup>5</sup>Phenome Health, Seattle, WA 98109, USA.

16 <sup>†</sup>Present address: Division of Public Health Sciences, Fred Hutchinson Cancer Research Center,  
17 Seattle, WA 98109, USA.

18 <sup>\*</sup>Correspondence to Noa Rappaport ([noa.rappaport@isbscience.org](mailto:noa.rappaport@isbscience.org))  
19

## 20 Abstract

21 Multiomic profiling can reveal population heterogeneity for both health and disease states. Obesity  
22 drives a myriad of metabolic perturbations in individuals and is a risk factor for multiple chronic  
23 diseases. Here, we report a global atlas of cross-sectional and longitudinal changes in 1,111 blood  
24 analytes associated with variation in Body Mass Index (BMI), as well as the multiomic associations  
25 with host polygenic risk scores and gut microbiome composition, from a cohort of 1,277 individuals  
26 enrolled in a wellness program. Machine learning model predictions of BMI from blood multiomics  
27 captured heterogeneous phenotypic states of host metabolism and gut microbiome composition, better  
28 than classically-measured BMI. Moreover, longitudinal analyses identified variable BMI trajectories  
29 for different omics measures in response to a healthy lifestyle intervention; metabolomics-inferred  
30 BMI decreased to a greater extent than actual BMI, while proteomics-inferred BMI exhibited greater  
31 resistance to change. Our analyses further revealed blood analyte–analyte associations that were  
32 significantly modified by metabolomics-inferred BMI and partially reversed in the metabolically  
33 obese population during the intervention. Taken together, our findings provide a blood atlas of the  
34 molecular perturbations associated with changes in obesity status, serving as a valuable resource to  
35 robustly quantify metabolic health for predictive and preventive medicine.  
36

## 37 Introduction

38 Obesity has been increasing in prevalence over the past four decades in adults, adolescents, and  
39 children around most of the world<sup>1,2</sup>. Many studies have demonstrated that obesity is a major risk  
40 factor for multiple chronic diseases such as type 2 diabetes mellitus (T2DM), metabolic syndrome  
41 (MetS), cardiovascular disease (CVD), and certain types of cancer<sup>3-6</sup>. In individuals with obesity, even  
42 a 5% loss in body weight can improve metabolic and cardiovascular health<sup>7</sup>, and weight loss through  
43 lifestyle interventions can reduce the risk for obesity-related chronic diseases<sup>8</sup>. Nevertheless, obesity  
44 and its physiological manifestations can vary widely across individuals, necessitating additional  
45 research to better understand this prevalent health condition.

46 Most commonly, obesity is quantified using the anthropometric Body Mass Index (BMI),  
47 defined as the body weight divided by body height squared [ $\text{kg m}^{-2}$ ]. While BMI does not directly  
48 measure body composition, BMI correlates well at the population level with direct measurements of  
49 body fat percentage using computed tomography (CT), magnetic resonance imaging (MRI), or dual-  
50 energy X-ray absorptiometry (DXA) (partial Pearson's  $r = 0.74-0.84$ )<sup>9</sup>. As an easily calculated and  
51 commonly understood measure among researchers, clinicians, and the general public, BMI is widely  
52 used for the primary diagnosis of obesity, and changes in BMI are often used to assess the efficacy of  
53 lifestyle interventions.

54 At the same time, there are considerable limitations to BMI as a surrogate measure of health  
55 state; e.g., differences in body composition can lead to misclassification of people with a high muscle-  
56 to-fat ratio (e.g., athletes) as the individual with obesity, and can undervalue metabolic improvements  
57 in health following exercise<sup>10</sup>. A meta-analysis showed that the common obesity diagnoses based on  
58 BMI cutoffs had high specificity but low sensitivity in identifying individuals with excess body fat<sup>11</sup>.  
59 The misclassification is likely due, in part, to the differences in BMI thresholds for obesity across  
60 different ethnic populations<sup>12</sup>, as well as the existence of a metabolically unhealthy, normal-weight  
61 (MUNW) group within the normal BMI class<sup>13,14</sup>. Likewise, there are health-heterogeneous groups  
62 among the individuals with obesity: metabolically healthy obese (MHO) and metabolically unhealthy  
63 obese (MUO). While most individuals in the MHO group are not necessarily healthy but simply  
64 healthier than individuals in the MUO group<sup>15</sup>, the transition from MHO to MUO phenotype may be a  
65 preceding step to the development of obesity-related chronic diseases<sup>16</sup>. Moreover, this transition is  
66 potentially preventable through lifestyle interventions<sup>17</sup>. Altogether, BMI is unequivocally useful at  
67 the population level, but too crude to capture a variety of heterogeneous metabolic health states.

68 Recent omics studies have demonstrated how blood omic profiles contain information  
69 relevant to a wide range of human health conditions; e.g., blood proteomics captured 11 health  
70 indicators such as the liver fat measured by ultrasound and the body composition measured by DXA<sup>18</sup>,  
71 while blood metabolomics tended to reflect dietary intake, lifestyle patterns, and gut microbiome  
72 profiles<sup>19,20</sup>. Intriguingly, a machine learning model that was trained to predict BMI using 49 BMI-  
73 associated blood metabolites captured obesity-related clinical measurements (e.g., insulin resistance,  
74 visceral fat percentage) better than observed BMI or genetic predisposition for high BMI<sup>21</sup>. Moreover,  
75 in a recent study on coronary artery disease, another blood metabolomics-based model of BMI  
76 efficiently reflected differences between individuals with or without acute coronary syndrome  
77 (ACS)<sup>22</sup>. Thus, while a single targeted metric (e.g., body composition) or a specific biomarker (e.g.,  
78 leptin, adiponectin<sup>23</sup>) provides useful information, multiomic blood profiling has the potential to  
79 comprehensively bridge the multifaceted gaps between BMI and heterogeneous physiological states.

80 In this study, we report heterogeneous molecular signatures of obesity by leveraging a cohort  
81 of 1,277 individuals with a wealth of phenotypic data, including human genomes and longitudinal  
82 measurements of metabolomics, proteomics, clinical laboratory tests, gut microbiomes, physical  
83 activity (i.e., wearables), and health/lifestyle questionnaires, and by employing machine learning to  
84 predict BMI. Blood-based analytes across all studied omics platforms exhibit strong performance in  
85 predicting measured BMI, explaining 48–78% of the variance in our main study cohort. We further  
86 show that multiomic phenotyping captures more refined levels of heterogeneity in metabolic states  
87 accompanying obesity, which is not apparent when using measured BMI. Moreover, longitudinal

88 analyses demonstrate variable changes in blood analytes across the studied omics platforms during a  
89 healthy lifestyle intervention; i.e., plasma metabolomics exhibited a stronger response to the  
90 intervention than measured BMI, while plasma proteomics exhibited a weaker response within a one-  
91 year span. Our findings highlight the utility and translational potential of blood multiomic profiling for  
92 investigating the complex molecular phenotypes underlying obesity and weight loss.  
93

## 94 Results

### 95 Plasma multiomics captured 48–78% of the variance in BMI

96 To investigate the molecular phenotypic perturbations associated with obesity, we selected a study  
97 cohort of 1,277 adults who participated in a scientific wellness program (Arivale)<sup>20,24–29</sup> and whose  
98 datasets included coupled measurements of plasma metabolomics, proteomics, and clinical laboratory  
99 tests from the same blood draw (Fig. 1a; see Methods). This study design allowed us to directly  
100 investigate the similarities and differences between omics platforms with regards to how they reflected  
101 the physiological health state of each individual across the BMI spectrum. This cohort was  
102 characteristically female (64.3%), middle-aged (mean  $\pm$  s.d.: 46.6  $\pm$  10.8 years), and white (69.7%)  
103 (Supplementary Fig. 1a–c, Supplementary Data 1). Based on the World Health Organization (WHO)  
104 international standards for BMI cutoffs (underweight:  $<18.5 \text{ kg m}^{-2}$ , normal:  $18.5\text{--}25 \text{ kg m}^{-2}$ ,  
105 overweight:  $25\text{--}30 \text{ kg m}^{-2}$ , obese:  $\geq 30 \text{ kg m}^{-2}$ )<sup>12</sup>, the baseline BMI prevalence was similar among  
106 normal, overweight, and obese classes, while only 0.8% of participants were in the underweight class  
107 (underweight: 10 participants (0.8%), normal: 426 participants (33.4%), overweight: 391 participants  
108 (30.6%), obese: 450 participants (35.2%)).

109 Leveraging the baseline measurements of plasma molecular analytes (766 metabolites, 274  
110 proteins, and 71 clinical laboratory tests; Supplementary Data 2), we trained machine learning models  
111 to predict baseline BMI (i.e., not forecast a future outcome but calculate an out-of-sample outcome)  
112 for each of the omics platforms (metabolomics, proteomics, and clinical labs) or in combination  
113 (combined omics of all metabolomics, proteomics, and clinical labs): metabolomics-based,  
114 proteomics-based, clinical labs (chemistries)-based, and combined omics-based BMI (MetBMI,  
115 ProtBMI, ChemBMI, and CombiBMI, respectively) models. To address multicollinearity among the  
116 analytes (Supplementary Fig. 2a) and to obtain predictions for all participants, we applied a tenfold  
117 iteration scheme of the least absolute shrinkage and selection operator (LASSO) algorithm with  
118 tenfold cross-validation (CV) (Fig. 1a; see Methods). This approach generated ten fitted sparse models  
119 for each omics category (Supplementary Data 3) and one single testing (hold-out) set-derived  
120 prediction from each omics category for each participant. The resulting models retained (i.e., assigned  
121 non-zero  $\beta$ -coefficient to) 62 metabolites, 30 proteins, 20 clinical laboratory tests, and 132 analytes  
122 across all ten MetBMI, ProtBMI, ChemBMI, and CombiBMI models, respectively, which exhibited  
123 low collinearity (Supplementary Fig. 2b, c) as expected from the LASSO algorithm<sup>30</sup>. In contrast to a  
124 model including obesity-related standard clinical measures (i.e., ordinary least squares (OLS) linear  
125 regression model with sex, age, triglycerides, high-density lipoprotein (HDL)-cholesterol, low-density  
126 lipoprotein (LDL)-cholesterol, glucose, insulin, and homeostatic model assessment for insulin  
127 resistance (HOMA-IR) as regressors; StandBMI model), each omics-based model demonstrated  
128 significantly higher performance in BMI prediction, ranging from out-of-sample  $R^2 = 0.48$   
129 (ChemBMI) to 0.70 (ProtBMI) compared to 0.37 (StandBMI) (Fig. 1b, c). The CombiBMI model  
130 exhibited the best performance in BMI prediction (out-of-sample  $R^2 = 0.78$ ; Fig. 1c), but the variances  
131 explained were not completely additive, suggesting that, although there is a considerable overlap in  
132 the signal detected by each omics platform, different omic measurements still contain non-redundant  
133 information regarding BMI. Additionally, these results were consistent in sex-stratified models, with  
134 the exception of male ChemBMI model that tended to exhibit higher performance than StandBMI  
135 model without statistical significance (Supplementary Fig. 2d).

136 To confirm the generalizability of our results, we investigated an external cohort of 1,834  
137 adults from the TwinsUK registry<sup>31</sup>, whose datasets included serum metabolomics<sup>32</sup> and the  
138 aforementioned standard clinical measures (Fig. 1a; see Methods). This external cohort was

139 demographically distinct from the Arivale cohort (Supplementary Fig. 1d–f, Supplementary Data 1);  
140 the TwinsUK cohort was overwhelmingly female (96.7%), senior (mean  $\pm$  s.d.: 61.4  $\pm$  9.0 years), and  
141 white (99.2%), and consisted of 15 (0.8%), 779 (42.5%), 706 (38.5%), and 334 (18.2%) participants in  
142 the underweight, normal, overweight, and obese BMI classes, respectively. To manage the differences  
143 in the metabolomics panels, we regenerated MetBMI models in the Arivale cohort, while restricting  
144 the metabolomic features to an overlapping set of 489 metabolites between the Arivale and TwinsUK  
145 panels (called restricted model). Although 25 of the retained metabolites in the original MetBMI  
146 models were replaced with other metabolites due to their absences in the restricted panel, 35 of the  
147 remaining 37 metabolites were consistently retained across the restricted MetBMI models  
148 (Supplementary Fig. 3a). Moreover,  $\beta$ -coefficients for the retained metabolites and MetBMI  
149 predictions for the Arivale cohort were consistent between the original and restricted models  
150 (Supplementary Fig. 3b, c). We then calculated BMI predictions for the TwinsUK cohort using the  
151 StandBMI and restricted MetBMI models that were fitted to the Arivale datasets. The restricted  
152 MetBMI model exhibited a lower absolute performance on the TwinsUK cohort compared to the  
153 Arivale cohort, but a significantly higher performance than StandBMI model (out-of-sample  $R^2 = 0.30$   
154 (MetBMI),  $-0.13$  (StandBMI); Fig. 1d, Supplementary Fig. 3d), confirming that blood metabolomics  
155 generally captures BMI better than the standard clinical measures.

156 BMI has been reported to be associated with multiple anthropometric and clinical measures,  
157 such as waist circumference (WC), blood pressure, sleep quality, and several polygenic risk scores  
158 (PRSs)<sup>3,4,15,27,33</sup>. Thus, we examined the association between the omics-inferred BMI and each of the  
159 available numeric physiological measures (see Methods; Supplementary Data 4). Among the 51  
160 assessed features, measured BMI was significantly associated with 27 features (false discovery rate  
161 (FDR)  $< 0.05$ ) including daily physical activity measures from wearable devices, waist-to-height ratio  
162 (WHtR), blood pressure, and BMI PRS (Fig. 1e). With minor differences in effect sizes, these BMI-  
163 associated features were concordantly associated with each omics-inferred BMI (Fig. 1e), indicating  
164 that the omics-inferred BMIs primarily maintain the characteristics of classical BMI in terms of  
165 anthropometric, genetic, lifestyle, and physiological associations.  
166

### 167 **Omics-based BMI estimates captured the variation in BMI better than any single analyte**

168 Because our LASSO linear regression model showed comparable performance to elastic net (EN) and  
169 ridge linear regression models and a non-linear random forest (RF) regression model (Supplementary  
170 Fig. 4a, b) and because LASSO model  $\beta$ -coefficients are generally easier to be interpreted, we chose  
171 to focus on the LASSO models. However, the LASSO algorithm randomly retains variables from  
172 highly collinear groups, and sets  $\beta$ -coefficients of the other variables to zero. To confirm the  
173 robustness of the variable selection process, we iterated the LASSO modeling while removing the  
174 strongest analyte (i.e., the analyte that had the highest absolute value for the mean of the ten  $\beta$ -  
175 coefficients) from the input omic dataset at the end of each iteration. If a variable is indispensable for  
176 a model, the performance should largely decrease after removing it. In all omics categories, a steep  
177 decay in the out-of-sample  $R^2$  was observed in the first 5–9 iterations (Supplementary Fig. 2e–h),  
178 suggesting that, at least, the top 5–9 variables that had the highest absolute  $\beta$ -coefficient values in the  
179 original LASSO models were indispensable for predicting BMI. Interestingly, the overall slope of  $R^2$   
180 in MetBMI model decayed more gradually compared to ProtBMI and ChemBMI models  
181 (Supplementary Fig. 2e–g), implying that metabolomics data contain more redundant information  
182 about BMI than the other omics data. Although larger number of metabolites in the input dataset  
183 might be a plausible explanation, the proportion of the variables that were robustly retained across all  
184 ten LASSO models (Supplementary Fig. 5) to the variables that were retained in at least one of the ten  
185 LASSO models was lower in MetBMI model compared to ProtBMI and ChemBMI models (MetBMI:  
186 62/209 metabolites  $\approx 30\%$ , ProtBMI: 30/74 proteins  $\approx 41\%$ , ChemBMI: 20/41 clinical laboratory tests  
187  $\approx 49\%$ ), confirming the higher level of redundancy within metabolomics data. Nevertheless,  
188 metabolites still constituted 58% of the 132 analytes that were retained across all ten CombiBMI  
189 models (77 metabolites, 51 proteins, 4 clinical laboratory tests; Fig. 2a), suggesting that each of the  
190 omics categories possesses unique information about BMI. The strongest predictors in CombiBMI

191 model were primarily proteins; e.g., analytes having the mean absolute  $\beta$ -coefficient  $> 0.02$  (i.e.,  
192 affecting more than  $\sim 2\%$  BMI in prediction per 1 s.d. of its change, according to the Taylor/Maclaurin  
193 series:  $e^\beta \approx 1 + \beta$  when  $\beta \ll 1$ ) were leptin (LEP), adrenomedullin (ADM), and fatty acid-binding  
194 protein 4 (FABP4) as the positive predictors and insulin-like growth factor-binding protein 1  
195 (IGFBP1) and advanced glycosylation end-product specific receptor (AGER; also described as  
196 receptor of AGE, RAGE) as the negative predictors. Note that these strongest proteins were consistent  
197 in the EN models (Supplementary Fig. 4c–f) and had high importance in the ridge and RF models  
198 (Supplementary Fig. 4g, h).

199 At the same time, the existence of these strong and consistently-retained predictors in the  
200 omics-based BMI models implied that a single analyte might be a suitable biomarker to predict BMI.  
201 To address this possibility, we regressed BMI independently on each of the analytes that were retained  
202 in at least one of the ten LASSO models (MetBMI: 209 metabolites, ProtBMI: 74 proteins,  
203 ChemBMI: 41 clinical laboratory tests; Supplementary Data 5). Among the analytes that were  
204 significantly associated with BMI (180 metabolites, 63 proteins, 30 clinical laboratory tests), only  
205 LEP, FABP4, and interleukin 1 receptor antagonist (IL1RN) exhibited over 30% of the explained  
206 variance in BMI by themselves (Fig. 2b–d), with a maximum of 37.9% variance explained (LEP). In  
207 contrast, MetBMI, ProtBMI, and ChemBMI models explained 68.9%, 70.6%, and 48.8% of the  
208 variance in BMI, respectively. Moreover, even upon eliminating several strong predictor analytes such  
209 as LEP and FABP4 from the omic datasets, the models still explained more variance in BMI than any  
210 single analyte (Supplementary Fig. 2e–h). These results indicate that the multiomic BMI prediction  
211 models explain a larger portion of the variation in BMI than any single analyte, and highlight the  
212 multivariate perturbation of blood analytes across all platforms with increasing BMI.  
213

#### 214 **Metabolic heterogeneity was responsible for the high rate of misclassification within the** 215 **standard BMI classes**

216 While the omics-inferred BMIs showed the similar phenotypic associations as the measured BMI (Fig.  
217 1e), we observed that the difference of the predicted BMI from the measured BMI ( $\Delta$ BMI) was highly  
218 correlated among the omics-based BMI models, ranging from Pearson's  $r = 0.64$  (ChemBMI vs.  
219 CombiBMI) to 0.83 (ProtBMI vs. CombiBMI) (Fig. 3a). In other words, the different omics  
220 consistently detected deviation of the omics-inferred BMI from the measured BMI per individual,  
221 implying that this deviation stemmed from a true biological signal of a perturbed physiological state  
222 rather than from noise or modeling artifacts. Actually, when individuals in the normal and obese BMI  
223 classes (defined by the WHO international standards) were subdivided by a clinical definition of  
224 metabolic health (i.e., defining metabolically unhealthy if having two or more MetS risks of the  
225 National Cholesterol Education Program (NCEP) Adult Treatment Panel III (ATP III) guidelines; see  
226 Methods)<sup>34,35</sup>,  $\Delta$ BMI was significantly higher in MUNW and MUO groups compared to metabolically  
227 healthy, normal-weight (MHNW) and MHO groups, respectively, for all omics categories (Fig. 3b),  
228 suggesting that the deviations of model predictions are related to metabolic health.

229 Nevertheless, there has been no universally accepted definition of metabolic health<sup>14,15,34,35</sup>.  
230 Thus, given the high interpretability and intuitiveness of the omics-inferred BMI, we further explored  
231 a potential application: using the omics-inferred BMI (instead of the measured BMI) for improved  
232 classification of both obesity and metabolic health with the WHO international standards. Each  
233 participant was classified using each of the measured and omics-inferred BMIs based on the standard  
234 BMI cutoffs, and categorized into either Matched or Mismatched group when the measured BMI class  
235 was matched or mismatched to each omics-inferred BMI class, respectively. The misclassification rate  
236 against the omics-inferred BMI class was  $\sim 30\%$  across all omics categories and BMI classes (Fig. 3c),  
237 consistent with the previously reported misclassification rates about the cardiometabolic health  
238 classification<sup>36,37</sup>. We then examined relationships between this omics-based misclassification within  
239 normal or obese BMI class and the obesity-related clinical blood markers (Supplementary Data 6),  
240 including triglycerides, HDL-cholesterol, LDL-cholesterol, high-sensitivity C-reactive protein (hs-  
241 CRP), glucose, insulin, HOMA-IR, glycated hemoglobin A1c (HbA1c), adiponectin, and vitamin

242 D<sup>3,15,23,38,39</sup>. Because ChemBMI and CombiBMI models were not independent of these markers, only  
243 the misclassification against MetBMI or ProtBMI class was examined in this analysis. The  
244 Mismatched group of normal BMI class exhibited significantly higher values of the markers that are  
245 positively associated with BMI (+BMI), such as triglycerides, hs-CRP, glucose, and HOMA-IR, and  
246 significantly lower values of the markers that are negatively associated with BMI (-BMI), such as  
247 HDL-cholesterol and adiponectin, compared to the Matched group of normal BMI class (FDR < 0.05;  
248 Fig. 3d). These patterns suggest that the participant misclassified into the normal BMI class possesses  
249 less healthy molecular profiles as similarly as the individual with overweight or obesity,  
250 corresponding to the individual with MUNW phenotype. Conversely, the Mismatched group of obese  
251 BMI class exhibited significantly lower and higher values of the positively and negatively BMI-  
252 associated markers, respectively, compared to the Matched group of obese BMI class (FDR < 0.05;  
253 Fig. 3d), suggesting that the participant misclassified as obese BMI class has healthier blood  
254 signatures, more similarly to the individual with overweight or normal-weight, corresponding to the  
255 individual with MHO phenotype. Likewise, we re-examined the 27 BMI-associated numeric  
256 physiological features (Fig. 1e, Supplementary Data 6), and found the concordant pattern of  
257 significant phenotypic differences between Matched and Mismatched groups in WHtR (+BMI), heart  
258 rate (+BMI), blood pressure (+BMI), and daily physical activity measures (-BMI) (FDR < 0.05; Fig. 3e).  
259 Importantly, there was no difference in BMI PRS (+BMI) between Matched and Mismatched groups  
260 (Fig. 3e), implying that lifestyle or environmental factors, rather than genetic risk, is likely involved in  
261 the discordance between the measured and omics-inferred BMIs. Furthermore, we validated and  
262 expanded these findings in the TwinsUK cohort:  $\Delta$ MetBMI was significantly higher in the  
263 metabolically unhealthy group compared to the metabolically healthy group within the normal BMI  
264 class (Supplementary Fig. 6a); the misclassification rate against MetBMI class was much higher  
265 (>60%) in the normal BMI class but ~30% in the others (Supplementary Fig. 6b); the concordant  
266 phenotypic differences between Matched and Mismatched groups were significantly observed in  
267 triglycerides (+BMI), HDL-cholesterol (-BMI), LDL-cholesterol (+BMI), hs-CRP (+BMI), and HOMA-IR  
268 (+BMI) (FDR < 0.05; Supplementary Fig. 6c). Remarkably, while DXA measurements were not  
269 performed in the Arivale cohort, the percentage of total fat in whole body (+BMI) and the ratio of fat in  
270 android region to fat in gynoid region (+BMI) were significantly higher in Mismatched group compared  
271 to Matched group within the normal BMI class of the TwinsUK cohort (FDR < 0.05; Supplementary  
272 Fig. 6c). Taken together, these results suggest that the omics-based BMI models can identify  
273 heterogeneous metabolic health states which are not captured by the measured BMI with the standard  
274 BMI cutoffs.  
275

## 276 **Metabolomics-inferred BMI reflected gut microbiome profiles better than BMI**

277 The gut microbiome has been shown to causally affect host obesity phenotypes in a mouse model<sup>40</sup>,  
278 and humans with obesity generally exhibit lower bacterial  $\alpha$ -diversity (i.e., the species richness and/or  
279 evenness of an ecological community)<sup>41,42</sup>. However, certain meta-analyses of human case-control  
280 studies suggest an inconsistent relationship between the gut microbiome and obesity<sup>43,44</sup>. Given our  
281 previous finding that the association between blood metabolites and bacterial diversity is dependent on  
282 BMI<sup>20</sup> and the current finding that the omics-based BMI models capture heterogeneous metabolic  
283 health states (Fig. 3), we hypothesized that MetBMI represents gut microbiome  $\alpha$ -diversity better than  
284 the measured BMI. For the 702 Arivale participants who had both stool-derived gut microbiome and  
285 blood omic datasets (Fig. 4a; see Methods), we examined relationships between gut microbiome  $\alpha$ -  
286 diversity (the number of observed species, Shannon's index, and Chao1 index) and the omics-based  
287 BMI misclassification. Matched and Mismatched groups against MetBMI class showed significant  
288 differences in all  $\alpha$ -diversity metrics within both normal and obese BMI classes (Fig. 4b), with the  
289 concordant pattern to the clinical markers and BMI-associated features (-BMI; e.g., HDL-cholesterol;  
290 Fig. 3d, e), implying that the MetBMI class reflects bacterial diversity better than BMI class.  
291 Interestingly, the misclassification against the other omics categories did not show these significant  
292 differences for all  $\alpha$ -diversity metrics and both BMI classes (Fig. 4b), consistent with our previous

293 observation that plasma metabolomics showed a much stronger correspondence to gut microbiome  
294 structure than either proteomics or clinical labs<sup>20</sup>.

295 We further examined the predictive power of gut microbiome profiles for MetBMI. For each  
296 of the measured BMI and MetBMI classes, we generated models classifying individuals into normal  
297 class versus obese class based on gut microbiome 16S rRNA gene amplicon sequencing data, using a  
298 fivefold iteration scheme of the RF algorithm with fivefold CV (Fig. 4a; see Methods). Compared to  
299 the classifier for the measured BMI class, the classifier for MetBMI class showed significantly larger  
300 area under curve (AUC) in the receiver operator characteristic (ROC) curve in the Arivale cohort  
301 (AUC = 0.66 (BMI), 0.75 (MetBMI); Fig. 4c), with significantly higher sensitivity and precision (Fig.  
302 4d). Moreover, by applying the same scheme to the stool-derived whole metagenomic shotgun  
303 sequencing (WMGS) data of the 329 TwinsUK participants<sup>45</sup> (Fig. 4a; see Methods), we validated that  
304 the gut microbiome-based obesity classifier for MetBMI class significantly outperformed the classifier  
305 for the measured BMI class in the TwinsUK cohort (AUC = 0.57 (BMI), 0.75 (MetBMI); Fig. 4e, f).  
306 Note that these classifiers were regenerated for the TwinsUK cohort (instead of using the classifiers  
307 that were fitted to the Arivale dataset; Fig. 4a) due to the difference in sequencing methods (amplicon  
308 sequencing vs. WMGS), while considering that the TwinsUK participants' MetBMIs were predicted  
309 from the Arivale-fitted MetBMI models (Fig. 1a). Altogether, these findings suggest that, although  
310 other factors (e.g., dietary intake<sup>19</sup>) may be involved, MetBMI has a stronger correspondence to gut  
311 microbiome features than the standard BMI.  
312

### 313 **Metabolic health of the metabolically obese group was substantially improved following a** 314 **healthy lifestyle intervention**

315 In the Arivale program, healthy lifestyle coaching was provided to all participants, resulting in clinical  
316 improvement across multiple measures of health<sup>25</sup>. This coaching intervention was personalized for  
317 each participant to improve the participant's health based on the combination of clinical laboratory  
318 tests, genetic predispositions, and published scientific evidence, and administered via telephone by  
319 registered dietitians, certified nutritionists, or registered nurses (see Methods and a previous report<sup>25</sup>).  
320 To investigate the longitudinal changes in omic profiles during the program, we defined a sub-cohort  
321 of 608 participants based on the available longitudinal measurements (Fig. 5a; see Methods). Given  
322 the participant-dependent variability in both count and time point of data collections, we estimated the  
323 average trajectory of each measured or omics-inferred BMI in the Arivale sub-cohort using a linear  
324 mixed model (LMM) with random effects for each participant (see Methods). Consistent with the  
325 previous analysis<sup>25,46</sup>, the mean BMI estimate for the overall cohort decreased during the program  
326 (Fig. 5b). The decrease of MetBMI was larger than that of measured BMI, while the decrease of  
327 ProtBMI was minimal and even smaller than that of measured BMI (Fig. 5b), suggesting that plasma  
328 metabolomics is highly responsive to the lifestyle intervention in the short term, while proteomics  
329 (measured from the same blood draw) is more resistant to change during the same intervention period.  
330 Subsequently, we generated LMMs with the baseline BMI class stratification, and confirmed that a  
331 significant decrease in the mean BMI estimate was observed in the overweight and obese BMI classes,  
332 but not in the normal BMI class (Fig. 5c). Concordantly, the mean estimates of ProtBMI and  
333 ChemBMI exhibited negative changes over time in the overweight and obese BMI classes, but not in  
334 the normal BMI class (Fig. 5c). In contrast, the mean estimate of MetBMI exhibited a significant  
335 decrease across all BMI classes (Fig. 5c), suggesting that metabolomics data captures information  
336 about the metabolic health response to the lifestyle intervention, beyond the baseline BMI class and  
337 the changes in BMI and other omic profiles.

338 Given the existence of multiple metabolic health sub-states within the standard BMI classes  
339 (Fig. 3), we further investigated the difference between misclassification strata against the baseline  
340 MetBMI class. In the (baseline) normal BMI class, while the mean estimate of the measured BMI  
341 remained constant in both Matched and Mismatched groups, the mean MetBMI estimate exhibited  
342 larger reduction in Mismatched group than Matched group (Fig. 5d), suggesting that the participants  
343 with MUNW phenotype improved their metabolic health to a greater extent than the participants with

344 MHNW phenotype. Likewise, in the (baseline) obese BMI class, while the decrease in the mean  
345 estimate of the measured BMI was not significantly different between Matched and Mismatched  
346 groups at one year after the enrollment, the decrease in the mean MetBMI estimate was larger in  
347 Matched group than in Mismatched group (Fig. 5e), suggesting that the participants with MUO  
348 phenotype improved their metabolic health to a greater extent than the participants with MHO  
349 phenotype. Altogether, these results suggest that metabolic health was substantially improved during  
350 the program, in accordance with an individual's baseline metabolomic state, rather than with the  
351 individual's baseline BMI class.  
352

### 353 **Plasma analyte correlation network in the metabolically obese group shifted toward a structure** 354 **observed in metabolically healthier state following a healthy lifestyle intervention**

355 We explored longitudinal changes in plasma analyte correlation networks, focusing on the  
356 metabolically obese group. Based on the importance of the baseline metabolomic state (Fig. 5d, e), we  
357 first assessed relationships between each plasma analyte–analyte correlation and the baseline MetBMI  
358 within the Arivale sub-cohort (Fig. 5a; 608 participants), using their interaction term in a generalized  
359 linear model (GLM; see Methods) of each analyte–analyte pair. In this type of model, the statistical  
360 test assesses whether the relationship between any two analytes is dependent on a third variable (in  
361 this case, the baseline MetBMI). Among 608,856 pairwise relationships of plasma analytes, 100  
362 analyte–analyte correlation pairs, comprising 82 metabolites, 33 proteins, and 16 clinical laboratory  
363 tests, were significantly modified by the baseline MetBMI (FDR < 0.05; Supplementary Data 7).  
364 Subsequently, we assessed longitudinal changes of these 100 pairs within the metabolically obese  
365 group (i.e., the baseline obese MetBMI class; 182 participants), using the interaction term (i.e.,  
366 interaction with days in the program) in a generalized estimating equation (GEE; see Methods) of each  
367 analyte–analyte pair. Among the 100 pairs, 27 analyte–analyte correlation pairs were significantly  
368 modified by days in the program (FDR < 0.05; Fig. 6a, Supplementary Data 7). These 27 pairs were  
369 mainly derived from metabolites (21 metabolites, 3 proteins, 3 clinical laboratory tests). One of these  
370 time-varying pairs was homoarginine and phenyllactate (PLA). Homoarginine was recently found to  
371 be a biomarker for CVD<sup>47</sup> and was a robustly retained positive predictor in MetBMI and CombiBMI  
372 models (Fig. 2a, Supplementary Fig. 5a). PLA is a gut microbiome-derived phenylalanine derivative  
373 known to have antimicrobial activity and antioxidant activity<sup>48,49</sup>. The positive correlation between  
374 homoarginine and PLA was observed in the metabolically obese group at baseline (Fig. 6b) and  
375 became weaker in this group during the course of the intervention (Fig. 6c), implying that metabolic  
376 dysregulation specific to the metabolically obese group was somewhat improved during the program.  
377 Collectively, these findings indicate that metabolic improvement was not limited to changes in  
378 specific blood analyte concentrations but also changes in the association structure among analytes.  
379

## 380 **Discussion**

381 Obesity is a significant risk factor for many chronic diseases<sup>3–6</sup>. The heterogeneous nature of human  
382 health conditions, with variable manifestation ranging from metabolic abnormalities to cardiovascular  
383 symptoms, calls for deeper molecular characterizations in order to optimize wellness and reduce the  
384 current global epidemic of chronic diseases. In this study, we have demonstrated that obesity  
385 profoundly perturbs human physiology, as reflected across all the studied omics modalities. The key  
386 findings of this study are: (1) machine learning-based multiomic BMI estimates were better suited to  
387 identifying heterogeneous metabolic health than the classically-measured BMI, while maintaining a  
388 high level of interpretability and intuitiveness attributed to the original metric (Fig. 1–3); (2) among  
389 all omics studied, metabolomic reflection of obesity exhibited the strongest correspondence to gut  
390 microbiome community structure (Fig. 4); (3) plasma metabolomics exhibited the strongest (and/or  
391 earliest) response to lifestyle coaching, while plasma proteomics exhibited a weaker (and/or more  
392 delayed) response than the measured BMI (Fig. 5b, c); (4) compared to the participants with  
393 metabolically healthy phenotype (i.e., BMI class = MetBMI class), the participants with metabolically  
394 unhealthy phenotype (i.e., BMI class < MetBMI class) exhibited a greater improvement in their



395 metabolic health (but not in weight loss per se) in response to the healthy lifestyle coaching (Fig. 5d,  
396 e); (5) dozens of analyte–analyte associations were modified in the participants of the metabolically  
397 obese group (i.e., obese MetBMI class), following the healthy lifestyle intervention (Fig. 6).

398 Although BMI is used as a measure of obesity, fat distribution in the body is an important  
399 factor for understanding the heterogeneous nature of obesity. In particular, abdominal obesity, which  
400 is characterized by excessive visceral fat (rather than subcutaneous fat) around the abdominal region,  
401 is known to be associated with chronic diseases such as MetS<sup>50</sup>. Thus, we addressed abdominal  
402 obesity by analyzing the anthropometric WHtR<sup>51,52</sup>, which was highly correlated with BMI in the  
403 Arivale sub-cohort (Pearson's  $r = 0.86$ ; Supplementary Fig. 7a–c). We generated omics-based WHtR  
404 models (Supplementary Fig. 7a, Supplementary Data 8), and obtained consistent findings to the  
405 omics-based BMI models (Supplementary Fig. 7d–m). Interestingly, the majority of the retained  
406 analytes in each omics-based WHtR model was also retained in its corresponding omics-based BMI  
407 model with the similar feature importance (Supplementary Fig. 8a–d). In addition,  $\Delta$ WHtR was highly  
408 correlated with  $\Delta$ BMI across all omics categories (Supplementary Fig. 8e). Moreover, although the  
409 WC measurements were not available for the defined TwinsUK cohort, direct fat measurements of the  
410 android region by DXA were associated with MetBMI class in the TwinsUK cohort (Supplementary  
411 Fig. 6c). Therefore, although BMI requires complementary information of the WC-related  
412 measurements for the diagnosis of abdominal obesity, the omics-based BMI model likely captures the  
413 obesity characteristics including abdominal obesity.

414 Multiple observational studies have explored obesity biomarkers. The involvements of  
415 insulin/insulin-like growth factor (IGF) axis and chronic low-grade inflammation have been discussed  
416 in the context of obesity-related disease risks<sup>5,6</sup>, backed up by robust associations of obesity with  
417 IGFBP1/2 ( $-$ BMI), adipokines such as LEP ( $+$ BMI), adiponectin ( $-$ BMI), FABP4 ( $+$ BMI), and ADM  
418 ( $+$ BMI), and proinflammatory cytokines such as interleukin 6 (IL6;  $+$ BMI)<sup>23,53</sup>. Consistent with these  
419 well-known associations, we observed positive BMI associations with LEP, FABP4, IL1RN, IL6,  
420 ADM, and insulin and negative BMI associations with IGFBP1/2 and adiponectin (Fig. 2c, d).  
421 Importantly, all these known biomarkers were incorporated into our omics-based BMI models, and  
422 most of them were consistently retained as important features of these models (Fig. 2a; Supplementary  
423 Fig. 5b, c). At the same time, we observed that RAGE explained a relatively small proportion of the  
424 variance in BMI (Fig. 2c), while being a strong negative predictive feature in all ten models of  
425 ProtBMI and CombiBMI (Fig. 2a, Supplementary Fig. 5b). Soluble RAGE (sRAGE) has been  
426 gradually highlighted in the contexts of T2DM and CVD<sup>54</sup>, with several reports on the negative  
427 association between sRAGE and BMI<sup>55</sup>. Therefore, omics-inferred BMI may reflect not only obesity  
428 status but also the early transition towards clinical manifestations of obesity-related chronic diseases.

429 Likewise, many epidemiological studies have revealed metabolomic biomarkers for  
430 obesity<sup>56,57</sup>. In line with these previous findings, we have confirmed positive BMI associations with  
431 mannose, uric acid (urate), and glutamate and negative BMI associations with asparagine and glycine  
432 (Fig. 2b). Furthermore, all of these metabolites were consistently incorporated into all ten models of  
433 MetBMI and CombiBMI (Fig. 2a, Supplementary Fig. 5a). In addition, many lipids emerged as strong  
434 predictors in MetBMI and CombiBMI models; in particular, glycerophosphocholines (GPCs) were  
435 negative predictors in these models, while sphingomyelins (SMs) were positive predictors (Fig. 2a,  
436 Supplementary Fig. 5a), even though both have a phosphocholine group in common. Although lipid  
437 has traditionally been regarded as a factor that is positively associated with obesity, recent  
438 metabolomics studies have revealed variable trends for different fatty acid species; e.g., plasma  
439 lysophosphatidylcholines (LPCs) are decreased in mice with obesity (high-fat diet model)<sup>58</sup>, which  
440 corresponded well with our results (e.g., LPC(18:1), described as 1-oleoyl-GPC(18:1) in Fig. 2b and  
441 Supplementary Fig. 5b). However, because there are many combinations of acyl residues in lipids and  
442 many potential confounding factors with obesity, systematic understanding of the species-level lipid  
443 biomarkers for obesity remains challenging<sup>56,57</sup>. Our approach, applying machine learning to  
444 metabolomics data, addresses this challenge by automatically and systematically providing a  
445 molecular signature of obesity, reflecting the versatile and complex metabolite species. Altogether,

446 omics-based BMI models can be regarded as multidimensional profiles of obesity, possessing detailed  
447 mechanistic information.

448 Recently, Cirulli and colleagues have reported a machine learning model for estimating BMI  
449 from blood metabolomics, which captured obesity-related phenotypes<sup>21</sup>. Their main model explained  
450 39.1% of the variance in BMI, while our MetBMI model explained 68.9% of the variance in BMI  
451 (Fig. 2b). Other than the difference in cohorts, the performance gap is likely a result of differences in  
452 modeling strategies. Cirulli and colleagues stringently selected 49 metabolites, out of their  
453 metabolomics panel of 1,007 metabolites, based on a pre-screening for significant adjusted-  
454 associations with BMI, and subsequently applied a tenfold CV implementation of ridge or LASSO  
455 method. In contrast, we used LASSO method for feature selection, applying it to our full  
456 metabolomics panel of 766 metabolites. In addition to the increased number of metabolites included in  
457 the model fitting, our higher performance may stem from the presence of metabolites which were  
458 critical for BMI prediction in a multivariate model, but not strongly associated with BMI on their own.  
459 Actually, similarly to the above example of RAGE in ProtBMI model, our MetBMI model contained  
460 multiple metabolites that were weakly associated with BMI but consistently retained across all ten  
461 models (Fig. 2b, Supplementary Fig. 5a). At the same time, the majority of the 49 metabolites reported  
462 by Cirulli and colleagues (14–20 metabolites among the 31–41 corresponding metabolites in our  
463 metabolomics panel) were retained in at least one of the ten MetBMI models. Therefore, our strategy  
464 of feature selection through machine learning, without a pre-filtering step, may be preferable for  
465 predicting BMI from metabolomics.

466 A recent study investigating multiomic changes in response to weight perturbations  
467 demonstrated that some weight gain-associated blood signatures were reversed during subsequent  
468 weight loss, while others persisted<sup>59</sup>. Interestingly, we found that MetBMI was more responsive to the  
469 healthy lifestyle intervention than the measured BMI or ChemBMI, while ProtBMI was more resistant  
470 to the same intervention (Fig. 5b, c). Our analyses of the predictors in the omics-based BMI models  
471 (Fig. 2; Supplementary Fig. 2e–h, 5) suggested that the distribution of feature importance among  
472 metabolites was considerably wider, while only a small subset of measured proteins (~5 proteins) was  
473 predominantly reflective of obesity profiles. Therefore, the effect of lifestyle coaching may consist of  
474 small additive contributions in blood metabolites in the short term. However, a longer longitudinal  
475 analysis is needed to infer the physiological meaning of these omics-dependent dynamics. For  
476 instance, it is possible that ProtBMI shows a delayed response to weight loss (over a span greater than  
477 a year measured presently; Fig. 5b, c), indicating blood metabolites and proteins may be early and late  
478 responders to a lifestyle intervention, respectively, such as in the case of the changes in blood glucose  
479 compared to the changes in HbA1c when assessing glucose homeostasis<sup>60</sup>. If the difference between  
480 the measured and omics-inferred BMIs remains constant even after one year, we would conclude that  
481 blood metabolites and proteins are more and less sensitive to weight loss than the measured BMI,  
482 respectively. In either scenario, monitoring blood multiomics during weight loss programs could help  
483 participants maintain their motivation to stay engaged with persistent lifestyle changes, because they  
484 would receive rapid feedback on how lifestyle changes were impacting their health, even in the  
485 absence of weight loss. In addition, long-term maintenance of the improvement is an important  
486 challenge for lifestyle interventions; although there is variability between prior reports, one study  
487 estimated that only ~20% of the individuals with overweight successfully maintain their weight loss in  
488 post-intervention<sup>61</sup>. Despite this relatively low rate of long-term success, there is evidence that  
489 lifestyle interventions had benefits in preventing diabetes incidence as far as 20 years post-  
490 intervention, even if weight was regained<sup>62,63</sup>. The observed larger improvement of MetBMI  
491 compared to the measured BMI could potentially contribute to this protective long-term effect,  
492 persisting even when weight is regained. Further investigation is required, especially with regard to  
493 the long-term dynamics of MetBMI and ProtBMI responses, which may provide a foothold in  
494 developing scientific strategies aimed at long-term maintenance of metabolic health.

495 Despite a number of highly promising findings, there were several limitations to our study.  
496 For example, this study was not designed as a randomized control trial, and we cannot strictly evaluate  
497 the effectiveness of the lifestyle intervention (e.g., bigger improvements in the obese group compared

498 to the normal-weight group may be due to the regression-toward-the-mean effect<sup>46</sup>). In addition, we  
499 used time as the variable in longitudinal analyses under an assumption that the program enrollment  
500 itself affected participant's BMI and omic profiles. However, if we had more detailed data on the  
501 intervention (e.g., magnitude, participants' compliance), we would be able to improve the assessment  
502 of its effect. The generalizability of our findings may be limited, because this study was an  
503 observational study of largely Caucasian cohorts from the Pacific West of the U.S. and from the U.K.  
504 and because validation with an external cohort relied on the female-dominated cohort (96.7%) and its  
505 metabolomics data. Our measurements did not cover all biomolecules in blood; in particular,  
506 proteomics was based on three targeted Olink panels. Thus, our findings on metabolomic and  
507 proteomic states are restricted to the analytes that we could measure. Nevertheless, this study will  
508 serve as a valuable resource for robustly characterizing metabolic health from the blood and  
509 identifying actionable targets for health management.  
510

## 511 **Methods**

### 512 **Study cohort**

513 The main study cohort (Arivale cohort) was derived from 6,223 individuals who participated in a  
514 wellness program offered by a currently closed commercial company (Arivale Inc., Washington,  
515 USA) between 2015–2019. An individual was eligible for enrollment if the individual was over 18  
516 years old, not pregnant, and a resident of any U.S. state except New York; participants were primarily  
517 recruited from Washington, California, and Oregon. The participants were not screened for any  
518 particular disease. During the Arivale program, each participant was provided personalized lifestyle  
519 coaching via telephone by registered dietitians, certified nutritionists, or registered nurses. This  
520 coaching was designed to improve the participant’s health based on the combination of clinical  
521 laboratory tests, genetic predispositions, and published scientific evidence; e.g., reduction of sodium  
522 intake might be recommended to any participants with high blood pressure, but if they also had risk  
523 alleles indicating enhanced susceptibility to dietary sodium, this risk would be emphasized (see a  
524 previous report<sup>25</sup> for more details). In the current study, to compare the associations between Body  
525 Mass Index (BMI) and host phenotypes across different omics, we limited the original cohort to the  
526 participants whose datasets contained (1) all main omic measurements (metabolomics, proteomics,  
527 clinical laboratory tests) from the same first blood draw, (2) a BMI measurement within  $\pm 1.5$  month  
528 from the first blood draw, and (3) genetic information (for using as covariates). We also eliminated (1)  
529 outlier participants whose baseline BMI was beyond  $\pm 3$  s.d. from the mean in the baseline BMI  
530 distribution and (2) participants whose any of omic datasets contained more than 10% missingness in  
531 the filtered analytes (see the next section). The final Arivale cohort consisted of 1,277 (821 female and  
532 456 male) participants (Fig. 1a), which exhibited consistent demographics (Supplementary Fig. 1a–c,  
533 Supplementary Data 1) with the study cohorts defined in the previous Arivale studies<sup>20,25–29</sup>. For the  
534 analyses of gut microbiome, sub-cohort was defined with the 702 (486 female and 216 male)  
535 participants from the Arivale cohort, who collected a stool sample within  $\pm 1.5$  month from the first  
536 blood draw and did not use antibiotics in the last three months (Fig. 4a, Supplementary Data 1). For  
537 longitudinal analyses, sub-cohort was defined with the 608 (410 female and 198 male) participants  
538 from the Arivale cohort, whose datasets contained two or more time-series datasets for both BMI and  
539 omics during 18 months after enrollment (Fig. 5a, Supplementary Data 1). For the analyses of waist-  
540 to-height ratio (WHtR), sub-cohort was defined with the 1,078 (689 female and 389 male) participants  
541 from the Arivale cohort, whose datasets contained the baseline WHtR measurement within  $\pm 1.5$   
542 month from the first blood draw and within  $\pm 3$  s.d. from the mean in the baseline WHtR distribution  
543 (Supplementary Fig. 7a, Supplementary Data 1).

544 The external cohort (TwinsUK cohort) was derived from 17,630 individuals who participated  
545 in the TwinsUK Registry, a British national register of adult twins<sup>31</sup>. Twins were recruited as  
546 volunteers by media campaigns without screening for any particular disease. The participants had two  
547 or more clinical visits for biological sampling between 1992–2022. In the current study, to validate  
548 our findings in the Arivale cohort, we limited the original cohort to the participants whose datasets  
549 contained all measurements for metabolomics<sup>32</sup>, BMI, and the obesity-related standard clinical  
550 measures (i.e., defined by triglycerides, high-density lipoprotein (HDL)-cholesterol, low-density  
551 lipoprotein (LDL)-cholesterol, glucose, insulin, and homeostatic model assessment for insulin  
552 resistance (HOMA-IR) throughout the current study) from the same visit. We also eliminated (1)  
553 outlier participants whose BMI was beyond  $\pm 3$  s.d. from the mean in the overall BMI distribution and  
554 (2) participants whose metabolomic dataset contained more than 10% missingness in the filtered  
555 metabolites (see the next section). The final TwinsUK cohort consisted of 1,834 (1,774 female and 60  
556 male) participants (Fig. 1a, Supplementary Fig. 1d–f, Supplementary Data 1). For the analyses of gut  
557 microbiome, sub-cohort was defined with the 329 (307 female and 22 male) participants from the  
558 TwinsUK cohort, who collected a stool sample within  $\pm 1.5$  month from the clinical visit and did not  
559 use antibiotics at that time (Fig. 4a, Supplementary Data 1).

560 The current study was conducted with de-identified data of the participants who had  
561 consented to the use of their anonymized data in research. All procedures were approved by the

562 Western Institutional Review Board (WIRB) with Institutional Review Board (IRB) (Study Number:  
563 20170658 at Institute for Systems Biology and 1178906 at Arivale) and by the TwinsUK Resource  
564 Executive Committee (TREC) (Project Number: E1192).  
565

## 566 **Data collections and data cleaning**

567 Multiomics data for the Arivale participants included genomics and longitudinal measurements of  
568 metabolomics, proteomics, clinical laboratory tests, gut microbiomes, wearable devices, and  
569 health/lifestyle questionnaires. Peripheral venous blood draws for all measurements were performed  
570 by trained phlebotomists at LabCorp (Laboratory Corporation of America Holdings, North Carolina,  
571 USA) or Quest (Quest Diagnostics, New Jersey, USA) service centers. Saliva to measure analytes  
572 such as diurnal cortisol and dehydroepiandrosterone (DHEA) was sampled by participants at home  
573 using a standardized kit (ZRT Laboratory, Oregon, USA). Likewise, stool samples for gut microbiome  
574 measurements were obtained by participants at home using a standardized kit (DNA Genotek, Inc.,  
575 Ottawa, Canada).

### 576 **– Genomics**

577 DNA was extracted from each whole blood sample and underwent whole genome sequencing  
578 (1,257 participants) or single-nucleotide polymorphisms (SNP) microarray genotyping (20  
579 participants). Genetic ancestry was calculated with principal components (PCs) using a set of  
580 ~100,000 ancestry-informative SNP markers, as described previously<sup>25</sup>. Polygenic risk scores  
581 (PRSs) were constructed using publicly available summary statistics from published genome-  
582 wide association studies (GWAS), as described previously<sup>27</sup>.  
583

### 584 **– Blood-measured omics**

585 Metabolomics data was generated by Metabolon, Inc. (North Carolina, USA), using ultra-  
586 high-performance liquid chromatography-tandem mass spectrometry (UHPLC-MS/MS) for  
587 plasma derived from each whole blood sample. Proteomics data was generated using  
588 proximity extension assay (PEA) for plasma derived from each whole blood sample with  
589 several Olink Target panels (Olink Proteomics, Uppsala, Sweden), and only the  
590 measurements with the Cardiovascular II, Cardiovascular III, and Inflammation panels were  
591 used in the current study since the other panels were not necessarily applied to all samples.  
592 All clinical laboratory tests were performed by LabCorp or Quest in a Clinical Laboratory  
593 Improvement Amendments (CLIA)-certified lab, and only the measurements by LabCorp  
594 were selected in the current study to eliminate potential differences between vendors. In the  
595 current study, the batch-corrected datasets with in-house pipeline were used, and  
596 metabolomic dataset was  $\log_e$ -transformed. In addition, analytes missing in more than 10% of  
597 the baseline samples were removed from each omic dataset, and observations missing in more  
598 than 10% of the remaining analytes were further removed. The final filtered metabolomics,  
599 proteomics, and clinical labs consisted of 766 metabolites, 274 proteins, 71 clinical laboratory  
600 tests, respectively (Supplementary Data 2).  
601

### 602 **– Gut microbiome**

603 Gut microbiome data was generated based on 16S amplicon sequencing of the V3+V4 region  
604 using a MiSeq sequencer (Illumina, Inc., California, USA) for DNA extracted from each stool  
605 sample, as previously described<sup>28</sup>. Briefly, the FASTQ files were processed using the mbtools  
606 workflow (<https://github.com/Gibbons-Lab/mbtools>) to remove noise, infer amplicon  
607 sequence variants (ASVs), and remove chimeras. Taxonomy assignment was performed using  
608 the SILVA ribosomal RNA gene database (version 132)<sup>64</sup>. In the current study, the final  
609 collapsed ASV table across the samples consisted of 394, 341, 85, 45, 26, and 16 taxa for  
610 species, genus, family, order, class, and phylum, respectively. Gut microbiome  $\alpha$ -diversity

611 was calculated at the ASV level using Shannon's index calculated by  $H = -\sum_{i=1}^S p_i \ln p_i$ ,  
612 where  $p_i$  is the proportion of a community  $i$  represented by ASVs, or using Chao1 diversity  
613 score calculated by  $S_{\text{Chao1}} = S_{\text{obs}} + \frac{n_1^2}{2n_2}$ , where  $S_{\text{obs}}$  is the number of observed ASVs,  $n_1$  is the  
614 number of singletons (ASVs captured once), and  $n_2$  is the number of doubletons (ASVs  
615 captured twice).  
616

#### 617 – Anthropometrics, saliva-measured analytes, and daily physical activity measures

618 Anthropometrics including weight, height, and waist circumference (WC) and blood pressure  
619 were measured at the time of blood draw and also reported by participants, which generated  
620 diverse timing and number of observations depending on each participant. BMI and WHtR  
621 were simultaneously calculated from the measured anthropometrics with the weight divided  
622 by squared height [ $\text{kg m}^{-2}$ ] and the WC divided by height [unitless], respectively.  
623 Measurements of saliva samples were performed in the testing laboratory of ZRT Laboratory.  
624 Daily physical activity measures such as heart rate, moving distance, step count, burned  
625 calories, floors climbed, and sleep quality were tracked using the Fitbit wearable device  
626 (Fitbit, Inc., California, USA). To manage variations between days, monthly averaged data  
627 was used for these daily measures. In the current study, the baseline measurement for these  
628 longitudinal measures was defined with the closest observation to the first blood draw per  
629 participant and data type, and each dataset was eliminated from analyses when its baseline  
630 measurement was beyond  $\pm 1.5$  month from the first blood draw.

631 Data resource for the TwinsUK participants included longitudinal measurements of metabolomics,  
632 clinical laboratory tests, dual-energy X-ray absorptiometry (DXA), and health/lifestyle  
633 questionnaires<sup>31</sup>. The necessary datasets for the current study were provided by Department of Twin  
634 Research & Genetic Epidemiology (King's College London). In the current study, after each provided  
635 dataset was cleaned as follows, the earliest visit among the visits from which all of metabolomics,  
636 BMI, and the standard clinical measures had been measured was defined as the baseline visit for each  
637 participant. As exception, the later visit among them was prioritized as the baseline visit, if the  
638 participant had gut microbiome data within  $\pm 1.5$  month from the visit. Only the baseline visit  
639 measurements were analyzed.

#### 640 – Blood-measured metabolomics

641 Metabolomics data was originally generated by Metabolon, Inc., using UHPLC-MS/MS for  
642 each serum sample<sup>32</sup>. In the current study, the provided median-normalized dataset was  $\log_e$ -  
643 transformed. In addition, metabolites missing in more than 10% of the overall samples were  
644 removed from metabolomic dataset, and observations missing in more than 10% of the  
645 remaining metabolites were further removed. The final filtered metabolomics consisted of  
646 683 metabolites.  
647

#### 648 – BMI

649 In the current study, the BMI values that had been already calculated and included in the  
650 provided metabolomics data file were used.  
651

#### 652 – Standard clinical measures and other phenotypic measures

653 In the current study, because the provided phenotypic datasets contained multiple  
654 measurements for a phenotype even from a single visit of a participant (e.g., due to project  
655 difference, repeated measurements), multiple measurements were flattened into a single  
656 measurement for a phenotype per each participant's visit by taking the mean value. During  
657 this flattening step, difference in unit was properly adjusted, and the value indicating below  
658 detection limit was regarded as zero. HOMA-IR was calculated from the datasets of glucose,

659 insulin, and fasting condition with the formula:  $\text{HOMA-IR} = \text{fasting glucose [mmol L}^{-1}] \times$   
660  $\text{fasting insulin [mIU L}^{-1}] \times 22.5^{-1}$ .  
661

## 662 – Gut microbiome

663 Gut microbiome data was originally generated based on whole metagenomic shotgun  
664 sequencing (WMGS) using a HiSeq 2500 sequencer (Illumina, Inc.) for DNA extracted from  
665 each stool sample<sup>45</sup>. In the current study, the raw sequencing data was obtained from the  
666 National Center for Biotechnology Information (NCBI) Sequence Read Archive (SRA)  
667 project (PRJEB32731), and applied to a processing pipeline ([https://github.com/Gibbons-](https://github.com/Gibbons-Lab/pipelines)  
668 [Lab/pipelines](https://github.com/Gibbons-Lab/pipelines)). Briefly, the obtained FASTQ files were processed using the fastp (version  
669 0.23.2) tool<sup>65</sup> to filter and trim the reads, and taxonomic abundance was obtained using the  
670 Kraken 2 (version 2.1.2) and Bracken (version 2.6.0) tools<sup>66</sup> with the Kraken 2 default  
671 database (based on NCBI RefSeq). The final collapsed taxonomic table across the samples  
672 consisted of 4,669, 1,225, 354, 167, 76, and 35 taxa for species, genus, family, order, class,  
673 and phylum, respectively.  
674

## 675 Blood omics-based BMI and WHtR models

676 For each Arivale baseline omic dataset, missing values were first imputed with a random forest (RF)  
677 algorithm using Python missingpy (version 0.2.0) library (corresponding to R MissForrest package<sup>67</sup>).  
678 For sex-stratified models (Supplementary Fig. 2d), the datasets after imputation were divided into sex-  
679 stratified datasets. Subsequently, the values in each omic dataset were standardized with Z-score using  
680 the mean and s.d. per analyte. Then, ten iterations of least absolute shrinkage and selection operator  
681 (LASSO) modeling with tenfold cross-validation (CV) (Fig. 1a, Supplementary Fig. 7a) were  
682 performed for the (unstandardized)  $\log_e$ -transformed BMI or WHtR and each processed omic dataset,  
683 using *LassoCV* application programming interface (API) of Python scikit-learn (version 1.0.1) library.  
684 Training and testing (hold-out) sets were generated by splitting participants into ten sets with one set  
685 as a testing (hold-out) set and the remaining nine sets as a training set, and iterating all combinations  
686 over those ten sets; i.e., overfitting was controlled using tenfold iteration with ten testing (hold-out)  
687 sets, and hyperparameter was decided using tenfold CV with internal training and validation sets from  
688 each training set. Consequently, this procedure generated ten fitted sparse models for each omics  
689 category (Supplementary Data 3) and one single testing (hold-out) set-derived prediction from each  
690 omics category for each participant. The same modeling scheme while replacing LASSO with elastic  
691 net (EN), ridge, or RF was performed using Python scikit-learn *ElasticNetCV*, *RidgeCV*, or  
692 *RandomForestRegressor*-implemented *GridSearchCV* API, respectively. In this RF-modeling, the  
693 number of trees in the forest and the number of features were set as the hyperparameters to be decided  
694 through CV. For the standard measures-based models, the above modeling scheme was applied to  
695 ordinary least squares (OLS) linear regression with sex, age, triglycerides, HDL-cholesterol, LDL-  
696 cholesterol, glucose, insulin, and HOMA-IR as regressors, using Python scikit-learn *LinearRegression*  
697 API. Of note, ten split sets were fixed among the omics categories and the modeling methods, and no  
698 significant difference in BMI, WHtR, sex, age, and ancestry PC1–5 among those ten sets was  
699 confirmed, using Pearson's  $\chi^2$  test for categorical variable and Analysis of Variance (ANOVA) for  
700 numeric variable while adjusting multiple testing with the Benjamini–Hochberg method across the  
701 tested variables (Supplementary Data 1).

702 For the TwinsUK cohort, metabolomic dataset was applied to RF imputation and then each  
703 dataset of metabolomics and the standard clinical measures was applied to Z-score standardization, as  
704 well as the Arivale datasets. Utilizing the ten LASSO or OLS linear regression models that were fitted  
705 by the Arivale dataset, one single prediction was calculated from each processed dataset for each  
706 participant by taking the mean of ten predicted values. For metabolomics, ten metabolomics-based  
707 BMI (MetBMI) models were regenerated while restricting the input Arivale metabolomics to the  
708 common 489 metabolites in the Arivale and TwinsUK panels (Supplementary Fig. 3).

709 For the LASSO-modeling iteration analysis (Supplementary Fig. 2e–h, 7f–i), ten LASSO  
710 models were repeatedly generated with the above modeling scheme. At the end of each iteration, the  
711 variable that was retained across ten models and that had the highest absolute value for the mean of  
712 ten  $\beta$ -coefficients was removed from the input omic dataset.

713 For longitudinal predictions of the Arivale sub-cohort, one single prediction at a time point  
714 was calculated from each processed time-series omic dataset for each participant, utilizing the baseline  
715 LASSO model for which the participant was included in the baseline testing (hold-out) set. This was  
716 because (1) the baseline measurements were minimally affected by the personalized lifestyle  
717 coaching, (2) both count and time point of data collections were different among the participants, and  
718 (3) potential data leakage might be derived from the relationships between the baseline and following  
719 measurements for the same participant. For processing, each time-series omic dataset was applied to  
720 two-step RF imputation, where the baseline missingness was first imputed based on the baseline data  
721 structure and the remaining missingness was next imputed based on the overall data structure, and  
722 subsequently applied to Z-score standardization using the mean and s.d. in the baseline distribution.

723 Model performance was conservatively evaluated by the out-of-sample  $R^2$  that was calculated  
724 from each corresponding hold-out testing set in the Arivale cohort or from the external testing set in  
725 the TwinsUK cohort. Pearson's  $r$  between the measured and predicted values was calculated from the  
726 overall participants of the Arivale or TwinsUK cohort. Difference of the predicted value from the  
727 measured value ( $\Delta$ Measure; i.e.,  $\Delta$ BMI or  $\Delta$ WhtR) was calculated with (the predicted value – the  
728 measured value)  $\times$  (the measured value) $^{-1} \times 100$  (i.e., the unit of  $\Delta$ Measure was [% Measure]). In the  
729 RF model, the importance of a feature was calculated as the normalized total reduction of the mean  
730 squared error that was brought by the feature.

731

### 732 **Health classification**

733 Each participant was classified using each of the measured and omics-inferred BMIs based on the  
734 World Health Organization (WHO) international standards for BMI cutoffs (underweight:  $<18.5 \text{ kg}$   
735  $\text{m}^{-2}$ , normal:  $18.5\text{--}25 \text{ kg m}^{-2}$ , overweight:  $25\text{--}30 \text{ kg m}^{-2}$ , obese:  $\geq 30 \text{ kg m}^{-2}$ )<sup>12</sup>. For the  
736 misclassification of BMI class against the omics-inferred BMI class, each participant was categorized  
737 into either Matched or Mismatched group when the measured BMI class was matched or mismatched  
738 to each omics-inferred BMI class, respectively.

739 For a clinically-defined metabolic health classification, the participants having two or more  
740 metabolic syndrome (MetS) risks of the National Cholesterol Education Program (NCEP) Adult  
741 Treatment Panel III (ATP III) guidelines were judged as the metabolically unhealthy group, while the  
742 other participants were judged as the metabolically healthy group<sup>34,35</sup>. Concretely, the MetS risk  
743 components were (1) systolic blood pressure  $\geq 130 \text{ mm Hg}$ , diastolic blood pressure  $\geq 85 \text{ mm Hg}$ , or  
744 using antihypertensive medication, (2) fasting triglyceride level  $\geq 150 \text{ mg dL}^{-1}$ , (3) fasting HDL-  
745 cholesterol level  $< 50 \text{ mg dL}^{-1}$  for female and  $< 40 \text{ mg dL}^{-1}$  for male or using lipid-lowering  
746 medication, and (4) fasting glucose level  $\geq 100 \text{ mg dL}^{-1}$  or using antidiabetic medication. Only the  
747 participants who had all these information were assessed in the corresponding analyses (Fig. 3b;  
748 Supplementary Fig. 6a, 7m).

749

### 750 **Gut microbiome-based models for classifying obesity**

751 For the Arivale gut microbiome dataset, the whole ASV table (907 taxa from species to phylum) was  
752 preprocessed (i.e., positively shifted by one,  $\log_e$ -transformed, and standardized with Z-score using the  
753 mean and s.d. per taxon) and then applied to dimensionality reduction using *PCA* API of Python  
754 scikit-learn (version 1.0.1) library; the projected values onto the first 50 PCs (0.4–5.1% variance  
755 explained) were supplied as the input gut microbiome features. Two types of classifiers were trained  
756 on these gut microbiome features: one predicting whether an individual is obese BMI class and the  
757 other predicting whether an individual is obese MetBMI class. Both models were independently  
758 constructed through a fivefold iteration scheme of RF with fivefold CV (Fig. 4a), using Python scikit-



759 learn *RandomForestClassifier*-implemented *GridSearchCV* API. In this RF-modeling, the number of  
760 trees in the forest and the number of features were set as the hyperparameters to be decided through  
761 CV. Training and testing (hold-out) sets were generated by splitting the participants of the normal and  
762 obese classes into five sets with one set as a testing (hold-out) set and the remaining four sets as a  
763 training set, and iterating all combinations over those five sets; i.e., overfitting was controlled using  
764 fivefold iteration with five testing (hold-out) sets, and hyperparameters were decided using fivefold  
765 CV with internal training and validation sets from each training set. Consequently, this procedure  
766 generated five fitted classifiers for each BMI or MetBMI class and one single testing (hold-out) set-  
767 derived prediction from each classifier type for each participant. Note that this prediction included two  
768 types: either normal or obese class by a vote of the trees (i.e., binary prediction) and the mean  
769 probability of obese class among the trees.

770 For the TwinsUK gut microbiome dataset, the whole taxonomic table (6,526 taxa from  
771 species to phylum) was preprocessed and then applied to dimensionality reduction, as well as the  
772 Arivale dataset; the projected values onto the first 50 PCs (0.2–40.1% variance explained) were  
773 supplied as the input gut microbiome features. Then, the five obesity classifiers for each BMI or  
774 MetBMI class were generated as well as the above Arivale procedure, and one single testing (hold-  
775 out) set-derived prediction from each classifier type was calculated for each participant (Fig. 4a).

776 Model performance of each classifier was conservatively evaluated using each corresponding  
777 hold-out testing set. Area under curve (AUC) in the receiver operator characteristic (ROC) curve and  
778 the average precision were calculated using the probability predictions, while sensitivity and  
779 specificity were calculated from confusion matrix using the binary predictions. The overall ROC  
780 curve and its AUC was calculated from all the participant's probability predictions, using R pROC  
781 (version 1.18.0) package<sup>68</sup>.

782

### 783 **Longitudinal changes in the measured and omics-inferred BMIs**

784 A linear mixed model (LMM) was generated for each  $\log_e$ -transformed measured or omics-inferred  
785 BMI in the Arivale sub-cohort, following the previous approach<sup>25</sup>. As fixed effects regarding time,  
786 linear regression splines with knots at 0, 6, 12, and 18 months were applied to days in program to fit  
787 time as a continuous variable rather than a categorical variable, because both count and time point of  
788 data collections were different among the participants. In addition to the linear regression splines of  
789 time as fixed effects, the LMM included sex, baseline age, ancestry PC1–5, and meteorological  
790 seasons as fixed effects (to adjust potential confounding effects) and random intercepts and random  
791 slopes of days in the program as random effects for each participant. Additionally, the same LMM for  
792 each measured or omics-inferred BMI was independently generated from each baseline BMI class-  
793 stratified group. Of note, this stratified LMM was not generated from the underweight group because  
794 its sample size was too small for convergence. For comparing difference between the misclassification  
795 strata against the baseline MetBMI class, the above LMM while adding additional fixed effects, the  
796 categorical baseline misclassification of BMI class against MetBMI class (i.e., binary for Matched vs.  
797 Mismatched) and its interaction terms with the linear regression splines of time, was generated for  
798 each measured BMI or MetBMI from each baseline BMI class-stratified group. All LMMs were  
799 modeled using *MixedLM* API of Python statsmodels (version 0.13.0) library.

800

### 801 **Plasma analyte correlation network analysis**

802 Prior to the analysis, outlier values which were beyond  $\pm 3$  s.d. from the mean in the Arivale sub-  
803 cohort baseline distribution were eliminated from the dataset per analyte, and seven clinical laboratory  
804 tests which became almost invariant across the participants were eliminated from analyses, allowing  
805 convergence in the following modeling. Per each analyte, values were converted with a transformation  
806 pipeline producing the lowest skewness (e.g., no transformation, the logarithm transformation for right  
807 skewed distribution, the square root transformation with mirroring for left skewed distribution) and  
808 standardized with *Z*-score using the mean and s.d.

809 Against 608,856 pairwise combinations of the analytes (766 metabolites, 274 proteomics, 64  
810 clinical laboratory tests), generalized linear models (GLMs) for the baseline measurements of the  
811 Arivale sub-cohort (Fig. 5a; 608 participants) were independently generated with the Gaussian  
812 distribution and identity link function using *glm* API of Python statsmodels (version 0.13.0) library.  
813 Each GLM consisted of an analyte as dependent variable, another analyte and the baseline MetBMI as  
814 independent variables with their interaction term, and sex, baseline age, and ancestry PC1–5 as  
815 covariates. The analyte–analyte correlation pair that was significantly modified by the baseline  
816 MetBMI was obtained based on the  $\beta$ -coefficient (two-sided *t*-test) of the interaction term between the  
817 independent variables in GLM, while adjusting multiple testing with the Benjamini–Hochberg method  
818 (false discovery rate (FDR) < 0.05).

819 Against the significant 100 pairs from the GLM analysis (82 metabolites, 33 proteins, and 16  
820 clinical laboratory tests; Supplementary Data 7), generalized estimating equations (GEEs) for the  
821 longitudinal measurements of the metabolically obese group (i.e., the baseline obese MetBMI class;  
822 182 participants) were independently generated with the exchangeable covariance structure using  
823 Python statsmodels *GEE* API. Each GEE consisted of an analyte as dependent variable, another  
824 analyte and days in the program as independent variables with their interaction term, and sex, baseline  
825 age, ancestry PC1–5, and meteorological seasons as covariates. The analyte–analyte correlation pair  
826 that was significantly modified by days in the program was obtained based on the  $\beta$ -coefficient (two-  
827 sided *t*-test) of the interaction term between the independent variables in GEE, while adjusting  
828 multiple testing with the Benjamini–Hochberg method (FDR < 0.05).  
829

### 830 **Statistical analysis**

831 All data preprocessing and statistical analyses were performed using Python NumPy (version 1.18.1 or  
832 1.21.3), pandas (version 1.0.3 or 1.3.4), SciPy (version 1.4.1 or 1.7.1) and statsmodels (version 0.11.1  
833 or 0.13.0) libraries, except for using R pROC (version 1.18.0) package<sup>68</sup> for DeLong’s test<sup>69</sup>. All  
834 statistical tests were performed using a two-sided hypothesis. In all cases of multiple testing, *P*-value  
835 was adjusted with the Benjamini–Hochberg method. Of note, because some hypotheses were not  
836 completely independent (e.g., between combined omics and each individual omics; between glucose,  
837 insulin, and HOMA-IR), this simple *P*-value adjustment was regarded as a conservative approach.  
838 Significance was based on *P* < 0.05 for single testing and FDR < 0.05 for multiple testing. Test  
839 summaries (e.g., sample size, degrees of freedom, test statistic, exact *P*-value) are found in  
840 Supplementary Data 4, 5, 6, 9, and 10.

841 Correlations (Fig. 1b, 3a; Supplementary Fig. 3b–d, 4b, 4f, 7c, 7d, 7l, 8d, 8e) were  
842 independently assessed using Pearson’s correlation test (Python SciPy *pearsonr* API), with the *P*-  
843 value adjustment if multiple testing. Comparisons of model performance (Fig. 1c, 1d, 4d, 4f;  
844 Supplementary Fig. 2d, 4a, 7e) were independently assessed using Welch’s *t*-test (Python statsmodels  
845 *ttest\_ind* API), with the *P*-value adjustment if multiple testing. Comparison of overall ROC curves  
846 (Fig. 4c, 4e) was assessed using unpaired DeLong’s test<sup>69</sup>.

847 In all regression analyses, only the baseline datasets were used, and, unless otherwise  
848 specified, all numeric variables were centered and scaled in advance. For the Arivale datasets of  
849 anthropometrics, saliva-measured analytes, daily physical activity measures, and PRSs, (1) outlier  
850 values which were beyond  $\pm 3$  s.d. from the mean in the cohort distribution were eliminated from the  
851 dataset per variable, (2) variables which became almost invariant across the participants were  
852 eliminated from the datasets, (3) values were converted with a transformation pipeline producing the  
853 lowest skewness (e.g., no transformation, the logarithm transformation for right skewed distribution,  
854 the square root transformation with mirroring for left skewed distribution), and (4) the transformed  
855 values were standardized with *Z*-score using the mean and s.d.; these preprocessed 51 variables were  
856 used as the numeric physiological features (Supplementary Data 4). Likewise, the Arivale datasets of  
857 the obesity-related clinical blood markers (i.e., selected clinical labs; Supplementary Data 6) and the  
858 TwinsUK datasets of the obesity-related phenotypic measures (Supplementary Data 6) were  
859 preprocessed. For gut microbiome  $\alpha$ -diversity metrics, the number of observed ASVs and Chao1

860 index were converted with square root transformation while Shannon's index was converted with  
861 square transformation, and then these transformed values were standardized with Z-score using the  
862 mean and s.d. Relationships of the numeric physiological features with the measured or omics-inferred  
863 BMI (Fig. 1e) were independently assessed using each OLS linear regression model with the  
864 (unstandardized)  $\log_e$ -transformed measured or omics-inferred BMI as dependent variable, a feature as  
865 independent variable, and sex, age, and ancestry PC1–5 as covariates, while adjusting multiple testing  
866 across the 255 (51 features  $\times$  5 BMI types) regressions. Relationships between Measure (i.e., BMI or  
867 WHtR) and the analytes that were retained in at least one of ten LASSO models (Fig. 2b–d,  
868 Supplementary Fig. 7k) were independently assessed using each OLS linear regression model with the  
869 (unstandardized)  $\log_e$ -transformed Measure as dependent variable, an analyte as independent variable,  
870 and sex, age, and ancestry PC1–5 as covariates, while adjusting multiple testing across the 210 (Fig.  
871 2b), 75 (Fig. 2c), 42 (Fig. 2d), or 289 (Supplementary Fig. 7k) regressions. In this regression analysis,  
872 a model including the omics-inferred Measure as independent variable was also assessed as reference.  
873 Differences in  $\Delta$ Measure (i.e.,  $\Delta$ BMI or  $\Delta$ WHtR) between clinically-defined metabolic health  
874 conditions (Fig. 3b; Supplementary Fig. 6a, 7m) were independently assessed using each OLS linear  
875 regression model with  $\Delta$ Measure as dependent variable, metabolic condition (i.e., Healthy vs.  
876 Unhealthy) as categorical independent variable, and Measure, sex, age, and ancestry PC1–5 as  
877 covariates, while adjusting multiple testing across the eight (two BMI classes  $\times$  four omics categories;  
878 Fig. 3b, Supplementary Fig. 7m) or four (two BMI classes  $\times$  two cohorts; Supplementary Fig. 6a)  
879 regressions. Differences in the obesity-related clinical blood markers, the BMI-associated numeric  
880 physiological features, or the gut microbiome  $\alpha$ -diversity metrics between the misclassification strata  
881 against the omics-inferred BMI class (Fig. 3d, 3e, 4b; Supplementary Fig. 6c) were independently  
882 assessed using each OLS linear regression model with a marker, feature, or metric as dependent  
883 variable, misclassification (i.e., Matched vs. Mismatched) as categorical independent variable, and  
884 BMI, sex, age, and ancestry PC1–5 as covariates, while adjusting multiple testing across the 40 (2  
885 BMI classes  $\times$  2 omics categories  $\times$  10 markers; Fig. 3d), 216 (2 BMI classes  $\times$  4 omics categories  $\times$   
886 27 features; Fig. 3e), 24 (2 BMI classes  $\times$  4 omics categories  $\times$  3 metrics; Fig. 4b), or 24 (2 BMI  
887 classes  $\times$  12 measures; Supplementary Fig. 6c) regressions. In the above regression analyses for the  
888 TwinsUK cohort, ancestry PCs were eliminated from the covariates due to data availability.  
889

## 890 Data visualization

891 Results were visualized using Python matplotlib (version 3.4.3) and seaborn (version 0.11.2) libraries,  
892 except for the plasma analyte correlation network. Data were summarized as the mean with 95%  
893 confidence interval (CI) or the boxplot (median: center line; 95% CI around median: notch;  $[Q_1, Q_3]$ :  
894 box limits;  $[x_{\min}, x_{\max}]$ : whiskers, where  $Q_1$  and  $Q_3$  are the 1st and 3rd quartile values, and  $x_{\min}$  and  $x_{\max}$   
895 are the minimum and maximum values in  $[Q_1 - 1.5 \times \text{IQR}, Q_3 + 1.5 \times \text{IQR}]$  (IQR: the interquartile  
896 range,  $Q_3 - Q_1$ ), respectively), as indicated in each figure legend. For presentation purpose, CI was  
897 simultaneously calculated during visualization using Python seaborn *barplot* or *boxplot* API with  
898 default setting (1,000 times bootstrapping or a Gaussian-based asymptotic approximation,  
899 respectively). The OLS linear regression line with 95% CI was simultaneously generated during  
900 visualization using Python seaborn *regplot* API with default setting (1,000 times bootstrapping). The  
901 plasma analyte correlation network was visualized with a circo plot using R circlize (version 0.4.15)  
902 package<sup>70</sup>.

## 903 Data availability

904 The de-identified Arivale datasets that were used in this study can be accessed by qualified researchers  
905 for research purposes. Requests should be sent to [data-access@isbscience.org](mailto:data-access@isbscience.org), and the data will be  
906 available after submission and approval of a research plan. The de-identified TwinsUK datasets that  
907 were used in this study were provided by Department of Twin Research & Genetic Epidemiology  
908 (King's College London) after the approval of our Data Access Application (Project Number: E1192).  
909

910 Requests should be referred to their website ([http://twinsuk.ac.uk/resources-for-researchers/access-](http://twinsuk.ac.uk/resources-for-researchers/access-our-data/)  
911 [our-data/](http://twinsuk.ac.uk/resources-for-researchers/access-our-data/)).

912

913 **Code availability**

914 Code used in this study is freely available on GitHub (<https://github.com/PriceLab/Multiomics-BMI>).

915

## 916 References

- 917 1. NCD Risk Factor Collaboration (NCD-RisC). Trends in adult body-mass index in 200 countries from 1975  
918 to 2014: a pooled analysis of 1698 population-based measurement studies with 19·2 million participants.  
919 *Lancet (London, England)* **387**, 1377–1396 (2016).
- 920 2. NCD Risk Factor Collaboration (NCD-RisC). Worldwide trends in body-mass index, underweight,  
921 overweight, and obesity from 1975 to 2016: a pooled analysis of 2416 population-based measurement  
922 studies in 128·9 million children, adolescents, and adults. *Lancet (London, England)* **390**, 2627–2642  
923 (2017).
- 924 3. Kopelman, P. G. Obesity as a medical problem. *Nature* **404**, 635–43 (2000).
- 925 4. Haslam, D. W. & James, W. P. T. Obesity. *Lancet (London, England)* **366**, 1197–209 (2005).
- 926 5. Kahn, S. E., Hull, R. L. & Utzschneider, K. M. Mechanisms linking obesity to insulin resistance and type 2  
927 diabetes. *Nature* **444**, 840–6 (2006).
- 928 6. Van Gaal, L. F., Mertens, I. L. & De Block, C. E. Mechanisms linking obesity with cardiovascular disease.  
929 *Nature* **444**, 875–80 (2006).
- 930 7. Magkos, F. *et al.* Effects of Moderate and Subsequent Progressive Weight Loss on Metabolic Function and  
931 Adipose Tissue Biology in Humans with Obesity. *Cell Metab.* **23**, 591–601 (2016).
- 932 8. Hamman, R. F. *et al.* Effect of weight loss with lifestyle intervention on risk of diabetes. *Diabetes Care* **29**,  
933 2102–7 (2006).
- 934 9. Sun, Q. *et al.* Comparison of dual-energy x-ray absorptiometric and anthropometric measures of adiposity in  
935 relation to adiposity-related biologic factors. *Am. J. Epidemiol.* **172**, 1442–54 (2010).
- 936 10. Prentice, A. M. & Jebb, S. A. Beyond body mass index. *Obes. Rev.* **2**, 141–7 (2001).
- 937 11. Okorodudu, D. O. *et al.* Diagnostic performance of body mass index to identify obesity as defined by body  
938 adiposity: A systematic review and meta-analysis. *Int. J. Obes.* **34**, 791–799 (2010).
- 939 12. WHO Expert Consultation. Appropriate body-mass index for Asian populations and its implications for  
940 policy and intervention strategies. *Lancet (London, England)* **363**, 157–63 (2004).
- 941 13. Ruderman, N., Chisholm, D., Pi-Sunyer, X. & Schneider, S. The metabolically obese, normal-weight  
942 individual revisited. *Diabetes* **47**, 699–713 (1998).
- 943 14. Ding, C., Chan, Z. & Magkos, F. Lean, but not healthy: the ‘metabolically obese, normal-weight’  
944 phenotype. *Curr. Opin. Clin. Nutr. Metab. Care* **19**, 408–417 (2016).
- 945 15. Smith, G. I., Mittendorfer, B. & Klein, S. Metabolically healthy obesity: facts and fantasies. *J. Clin. Invest.*  
946 **129**, 3978–3989 (2019).
- 947 16. Appleton, S. L. *et al.* Diabetes and cardiovascular disease outcomes in the metabolically healthy obese  
948 phenotype: a cohort study. *Diabetes Care* **36**, 2388–94 (2013).
- 949 17. Schröder, H. *et al.* Determinants of the transition from a cardiometabolic normal to abnormal  
950 overweight/obese phenotype in a Spanish population. *Eur. J. Nutr.* **53**, 1345–53 (2014).
- 951 18. Williams, S. A. *et al.* Plasma protein patterns as comprehensive indicators of health. *Nat. Med.* **25**, 1851–  
952 1857 (2019).
- 953 19. Bar, N. *et al.* A reference map of potential determinants for the human serum metabolome. *Nature* **588**, 135–  
954 140 (2020).
- 955 20. Wilmski, T. *et al.* Blood metabolome predicts gut microbiome  $\alpha$ -diversity in humans. *Nat. Biotechnol.* **37**,  
956 1217–1228 (2019).
- 957 21. Cirulli, E. T. *et al.* Profound Perturbation of the Metabolome in Obesity Is Associated with Health Risk. *Cell*  
958 *Metab.* **29**, 488–500.e2 (2019).
- 959 22. Talmor-Barkan, Y. *et al.* Metabolomic and microbiome profiling reveals personalized risk factors for  
960 coronary artery disease. *Nat. Med.* **28**, 295–302 (2022).
- 961 23. Nimptsch, K., Konigorski, S. & Pischon, T. Diagnosis of obesity and use of obesity biomarkers in science  
962 and clinical medicine. *Metabolism.* **92**, 61–70 (2019).
- 963 24. Price, N. D. *et al.* A wellness study of 108 individuals using personal, dense, dynamic data clouds. *Nat.*  
964 *Biotechnol.* **35**, 747–756 (2017).
- 965 25. Zubair, N. *et al.* Genetic Predisposition Impacts Clinical Changes in a Lifestyle Coaching Program. *Sci. Rep.*  
966 **9**, 6805 (2019).
- 967 26. Earls, J. C. *et al.* Multi-Omic Biological Age Estimation and Its Correlation With Wellness and Disease  
968 Phenotypes: A Longitudinal Study of 3,558 Individuals. *J. Gerontol. A. Biol. Sci. Med. Sci.* **74**, S52–S60  
969 (2019).
- 970 27. Wainberg, M. *et al.* Multiomic blood correlates of genetic risk identify presymptomatic disease alterations.  
971 *Proc. Natl. Acad. Sci. U. S. A.* **117**, 21813–21820 (2020).

- 972 28. Wilmanski, T. *et al.* Gut microbiome pattern reflects healthy ageing and predicts survival in humans. *Nat.*  
973 *Metab.* **3**, 274–286 (2021).
- 974 29. Zimmer, A. *et al.* The geometry of clinical labs and wellness states from deeply phenotyped humans. *Nat.*  
975 *Commun.* **12**, 3578 (2021).
- 976 30. Tibshirani, R. Regression Shrinkage and Selection Via the Lasso. *J. R. Stat. Soc. Ser. B* **58**, 267–288 (1996).
- 977 31. Moayyeri, A., Hammond, C. J., Valdes, A. M. & Spector, T. D. Cohort Profile: TwinsUK and healthy  
978 ageing twin study. *Int. J. Epidemiol.* **42**, 76–85 (2013).
- 979 32. Long, T. *et al.* Whole-genome sequencing identifies common-to-rare variants associated with human blood  
980 metabolites. *Nat. Genet.* **49**, 568–578 (2017).
- 981 33. Xu, X. *et al.* Habitual sleep duration and sleep duration variation are independently associated with body  
982 mass index. *Int. J. Obes. (Lond)*. **42**, 794–800 (2018).
- 983 34. Stefan, N., Schick, F. & Häring, H.-U. Causes, Characteristics, and Consequences of Metabolically  
984 Unhealthy Normal Weight in Humans. *Cell Metab.* **26**, 292–300 (2017).
- 985 35. Blüher, M. Metabolically Healthy Obesity. *Endocr. Rev.* **41**, 405–420 (2020).
- 986 36. Shah, N. R. & Braverman, E. R. Measuring adiposity in patients: the utility of body mass index (BMI),  
987 percent body fat, and leptin. *PLoS One* **7**, e33308 (2012).
- 988 37. Tomiyama, A. J., Hunger, J. M., Nguyen-Cuu, J. & Wells, C. Misclassification of cardiometabolic health  
989 when using body mass index categories in NHANES 2005-2012. *Int. J. Obes. (Lond)*. **40**, 883–6 (2016).
- 990 38. Bennett, C. M., Guo, M. & Dharmage, S. C. HbA(1c) as a screening tool for detection of Type 2 diabetes: a  
991 systematic review. *Diabet. Med.* **24**, 333–43 (2007).
- 992 39. Pereira-Santos, M., Costa, P. R. F., Assis, A. M. O., Santos, C. A. S. T. & Santos, D. B. Obesity and vitamin  
993 D deficiency: a systematic review and meta-analysis. *Obes. Rev.* **16**, 341–9 (2015).
- 994 40. Ridaura, V. K. *et al.* Gut microbiota from twins discordant for obesity modulate metabolism in mice.  
995 *Science* **341**, 1241214 (2013).
- 996 41. Turnbaugh, P. J. *et al.* A core gut microbiome in obese and lean twins. *Nature* **457**, 480–484 (2009).
- 997 42. Le Chatelier, E. *et al.* Richness of human gut microbiome correlates with metabolic markers. *Nature* **500**,  
998 541–546 (2013).
- 999 43. Walters, W. A., Xu, Z. & Knight, R. Meta-analyses of human gut microbes associated with obesity and IBD.  
1000 *FEBS Lett.* **588**, 4223–4233 (2014).
- 1001 44. Duvallet, C., Gibbons, S. M., Gurry, T., Irizarry, R. A. & Alm, E. J. Meta-analysis of gut microbiome  
1002 studies identifies disease-specific and shared responses. *Nat. Commun.* **8**, 1784 (2017).
- 1003 45. Visconti, A. *et al.* Interplay between the human gut microbiome and host metabolism. *Nat. Commun.* **10**,  
1004 4505 (2019).
- 1005 46. Diener, C. *et al.* Baseline Gut Metagenomic Functional Gene Signature Associated with Variable Weight  
1006 Loss Responses following a Healthy Lifestyle Intervention in Humans. *mSystems* **6**, e0096421 (2021).
- 1007 47. Karetnikova, E. S. *et al.* Is Homoarginine a Protective Cardiovascular Risk Factor? *Arterioscler. Thromb.*  
1008 *Vasc. Biol.* **39**, 869–875 (2019).
- 1009 48. Dieuleveux, V., Lemarinier, S. & Guéguen, M. Antimicrobial spectrum and target site of D-3-phenyllactic  
1010 acid. *Int. J. Food Microbiol.* **40**, 177–83 (1998).
- 1011 49. Beloborodova, N. *et al.* Effect of phenolic acids of microbial origin on production of reactive oxygen  
1012 species in mitochondria and neutrophils. *J. Biomed. Sci.* **19**, 89 (2012).
- 1013 50. Després, J.-P. & Lemieux, I. Abdominal obesity and metabolic syndrome. *Nature* **444**, 881–7 (2006).
- 1014 51. Ashwell, M., Gunn, P. & Gibson, S. Waist-to-height ratio is a better screening tool than waist circumference  
1015 and BMI for adult cardiometabolic risk factors: systematic review and meta-analysis. *Obes. Rev.* **13**, 275–86  
1016 (2012).
- 1017 52. Swainson, M. G., Batterham, A. M., Tsakirides, C., Rutherford, Z. H. & Hind, K. Prediction of whole-body  
1018 fat percentage and visceral adipose tissue mass from five anthropometric variables. *PLoS One* **12**, e0177175  
1019 (2017).
- 1020 53. Li, Y. *et al.* Adrenomedullin is a novel adipokine: adrenomedullin in adipocytes and adipose tissues.  
1021 *Peptides* **28**, 1129–43 (2007).
- 1022 54. Egaña-Gorroño, L. *et al.* Receptor for Advanced Glycation End Products (RAGE) and Mechanisms and  
1023 Therapeutic Opportunities in Diabetes and Cardiovascular Disease: Insights From Human Subjects and  
1024 Animal Models. *Front. Cardiovasc. Med.* **7**, 37 (2020).
- 1025 55. Norata, G. D. *et al.* Circulating soluble receptor for advanced glycation end products is inversely associated  
1026 with body mass index and waist/hip ratio in the general population. *Nutr. Metab. Cardiovasc. Dis.* **19**, 129–  
1027 34 (2009).

- 1028 56. Rauschert, S., Uhl, O., Koletzko, B. & Hellmuth, C. Metabolomic biomarkers for obesity in humans: A  
1029 short review. *Ann. Nutr. Metab.* **64**, 314–324 (2014).
- 1030 57. Rangel-Huerta, O. D., Pastor-Villaescusa, B. & Gil, A. Are we close to defining a metabolomic signature of  
1031 human obesity? A systematic review of metabolomics studies. *Metabolomics* **15**, 93 (2019).
- 1032 58. Barber, M. N. *et al.* Plasma lysophosphatidylcholine levels are reduced in obesity and type 2 diabetes. *PLoS*  
1033 *One* **7**, e41456 (2012).
- 1034 59. Piening, B. D. *et al.* Integrative Personal Omics Profiles during Periods of Weight Gain and Loss. *Cell Syst.*  
1035 **6**, 157–170.e8 (2018).
- 1036 60. Koenig, R. J. *et al.* Correlation of glucose regulation and hemoglobin A1c in diabetes mellitus. *N. Engl. J.*  
1037 *Med.* **295**, 417–20 (1976).
- 1038 61. Wing, R. R. & Phelan, S. Long-term weight loss maintenance. *Am. J. Clin. Nutr.* **82**, 222S–225S (2005).
- 1039 62. Li, G. *et al.* The long-term effect of lifestyle interventions to prevent diabetes in the China Da Qing Diabetes  
1040 Prevention Study: a 20-year follow-up study. *Lancet (London, England)* **371**, 1783–9 (2008).
- 1041 63. Diabetes Prevention Program Research Group *et al.* 10-year follow-up of diabetes incidence and weight loss  
1042 in the Diabetes Prevention Program Outcomes Study. *Lancet (London, England)* **374**, 1677–86 (2009).
- 1043 64. Yilmaz, P. *et al.* The SILVA and ‘All-species Living Tree Project (LTP)’ taxonomic frameworks. *Nucleic*  
1044 *Acids Res.* **42**, D643–8 (2014).
- 1045 65. Chen, S., Zhou, Y., Chen, Y. & Gu, J. fastp: an ultra-fast all-in-one FASTQ preprocessor. *Bioinformatics*  
1046 **34**, i884–i890 (2018).
- 1047 66. Lu, J. *et al.* Metagenome analysis using the Kraken software suite. *Nat. Protoc.* 1–25 (2022).  
1048 doi:10.1038/s41596-022-00738-y
- 1049 67. Stekhoven, D. J. & Bühlmann, P. Missforest-Non-parametric missing value imputation for mixed-type data.  
1050 *Bioinformatics* **28**, 112–118 (2012).
- 1051 68. Robin, X. *et al.* pROC: an open-source package for R and S+ to analyze and compare ROC curves. *BMC*  
1052 *Bioinformatics* **12**, 77 (2011).
- 1053 69. DeLong, E. R., DeLong, D. M. & Clarke-Pearson, D. L. Comparing the areas under two or more correlated  
1054 receiver operating characteristic curves: a nonparametric approach. *Biometrics* **44**, 837–45 (1988).
- 1055 70. Gu, Z., Gu, L., Eils, R., Schlesner, M. & Brors, B. Circlize implements and enhances circular visualization  
1056 in R. *Bioinformatics* **30**, 2811–2812 (2014).
- 1057

1058 **Acknowledgements**

1059 We thank Sergey A. Kornilov, Gustavo Glusman, and Max Robinson (Institute for Systems Biology;  
1060 ISB) for providing comments to this study. We thank Victoria Vazquez and Andrew Anastasiou  
1061 (King's College London) for their support in obtaining and utilizing the TwinsUK data access. We are  
1062 grateful to all Arivale and TwinsUK participants who consented to using their deidentified data for  
1063 research purposes. This work was supported by the M.J. Murdock Charitable Trust (Reference No.  
1064 2014096:MNL:11/20/2014, awarded to N.D.P. and L.H.), the National Institutes of Health (NIH)  
1065 grants awarded by the National Institute on Aging (NIA) (U19AG023122 and 5U01AG061359), and a  
1066 generous gift from K. Carole Ellison (to K.W., T.W., and A.Z.). K.W. was supported by The Uehara  
1067 Memorial Foundation (Overseas Postdoctoral Fellowships). C.D. and S.M.G. were supported by the  
1068 Washington Research Foundation Distinguished Investigator Award and startup funds from ISB.  
1069 TwinsUK is funded by the Wellcome Trust, Medical Research Council, Versus Arthritis, European  
1070 Union Horizon 2020, Chronic Disease Research Foundation (CDRF), Zoe Ltd, the National Institute  
1071 for Health and Care Research (NIHR) Clinical Research Network (CRN) and Biomedical Research  
1072 Centre based at Guy's and St Thomas' NHS Foundation Trust in partnership with King's College  
1073 London.  
1074

1075 **Author Contribution**

1076 K.W., T.W., L.H., N.D.P., and N.R. conceptualized the study. K.W., T.W., A.Z., N.D.P., and N.R.  
1077 participated in the study design. K.W., T.W., C.D., B.L., and N.R. performed data analysis and figure  
1078 generation. C.D., J.C.E., J.J.H., J.C.L., S.M.G., A.T.M., and L.H. assisted in results interpretation.  
1079 J.C.L. and A.T.M. managed the logistics of data collection and integration. K.W., T.W., and N.R.  
1080 were the primary authors of the paper, with contributions from all other authors. All authors read and  
1081 approved the final manuscript.  
1082

1083 **Competing Interests**

1084 J.J.H. has received grants from Pfizer and Novartis for research unrelated to this study. All other  
1085 authors declare no competing interests.  
1086



1087 **Figures**

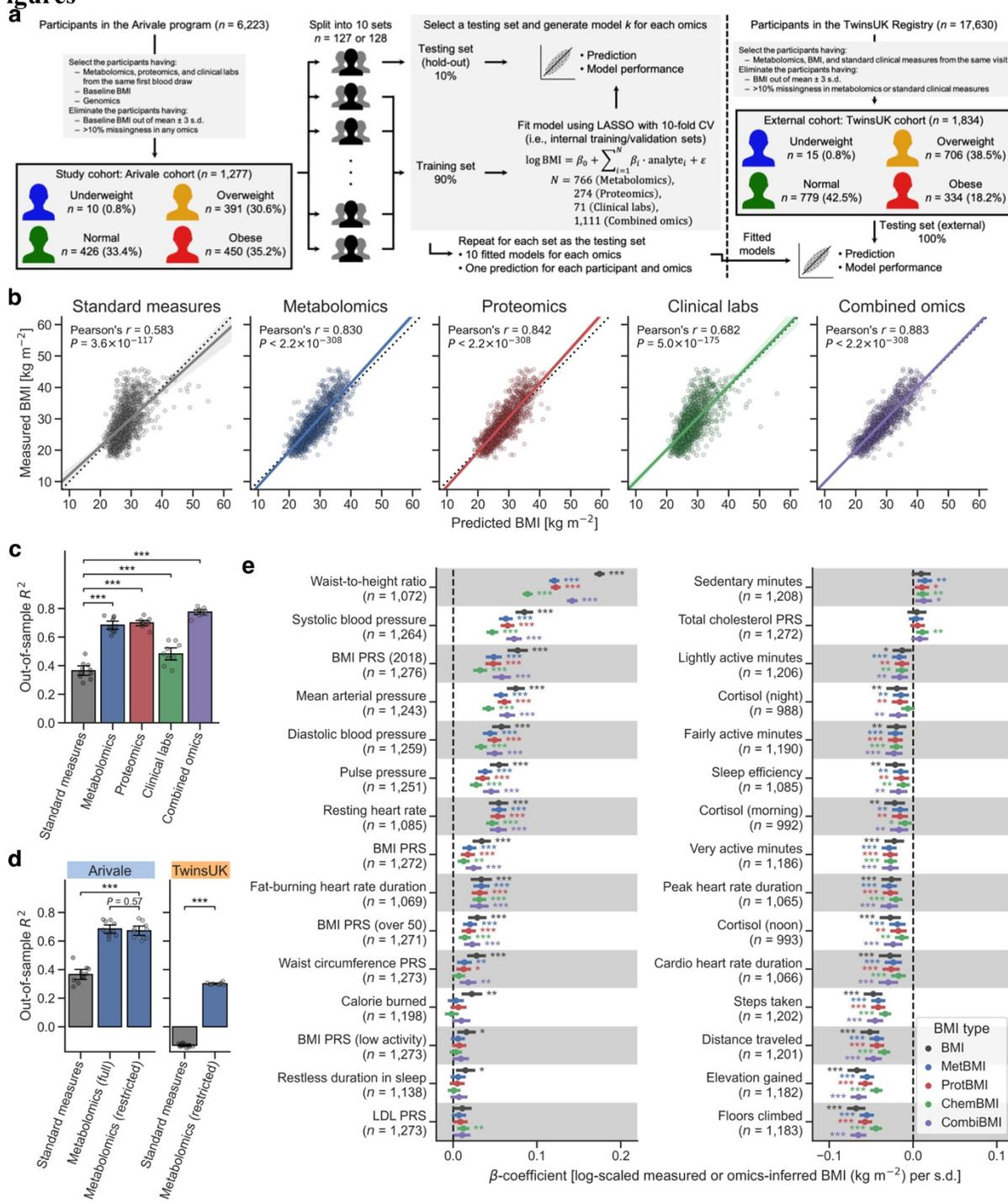


**Figure 1. Plasma multiomics captured 48–78% of the variance in BMI.**

1088  
 1089  
 1090 **a** Overview of study cohorts and the omics-based Body Mass Index (BMI) model generation. LASSO:  
 1091 least absolute shrinkage and selection operator, CV: cross-validation. **b** Correlation between the  
 1092 measured and predicted BMIs. The solid line is the ordinary least squares (OLS) linear regression line  
 1093 with 95% confidence interval (CI), and the dotted line is measured BMI = predicted BMI. Standard  
 1094 measures: OLS linear regression model with sex, age, triglycerides, high-density lipoprotein (HDL)-  
 1095 cholesterol, low-density lipoprotein (LDL)-cholesterol, glucose, insulin, and homeostatic model

1096 assessment for insulin resistance (HOMA-IR) as regressors;  $P$ : adjusted  $P$ -value of two-sided  
1097 Pearson's correlation test with the Benjamini–Hochberg method across the five categories.  $n = 1,277$   
1098 participants. **c, d** Model performance of each fitted BMI model. Out-of-sample  $R^2$  was calculated from  
1099 each corresponding hold-out testing set (**c**, Arivale in **d**) or from the external testing set (TwinsUK in  
1100 **d**). Metabolomics (full): LASSO model trained by all 766 metabolites of the Arivale dataset,  
1101 Metabolomics (restricted): LASSO model trained by the common 489 metabolites in the Arivale and  
1102 TwinsUK datasets (see Supplementary Fig. 3). Note that Standard measures and Metabolomics (full)  
1103 of Arivale in **d** are the same with corresponding ones in **c**. Data: mean with 95% CI,  $n = 10$  models.  
1104 \*\*\*Adjusted  $P < 0.001$  in two-sided Welch's  $t$ -test with the Benjamini–Hochberg method across the  
1105 four (**c**) or three (**d**) comparisons. **e** Association between omics-inferred BMI and physiological  
1106 feature. For each of the 51 numeric physiological features (Supplementary Data 4),  $\beta$ -coefficient was  
1107 estimated using OLS linear regression model with the measured or omics-inferred BMI as dependent  
1108 variable and sex, age, and ancestry principal components (PCs) as covariates. Presented are the 30  
1109 features that were significantly associated with at least one of the BMI types after multiple testing  
1110 adjustment with the Benjamini–Hochberg method across the 255 (51 features  $\times$  5 BMI types)  
1111 regressions. BMI: measured BMI, MetBMI: metabolomics-inferred BMI, ProtBMI: proteomics-  
1112 inferred BMI, ChemBMI: clinical chemistries-inferred BMI, CombiBMI: combined omics-inferred  
1113 BMI, PRS: polygenic risk score,  $n$ : the number of assessed participants. Data: estimate with 95% CI.  
1114 \*Adjusted  $P < 0.05$ , \*\*adjusted  $P < 0.01$ , \*\*\*adjusted  $P < 0.001$ .  
1115

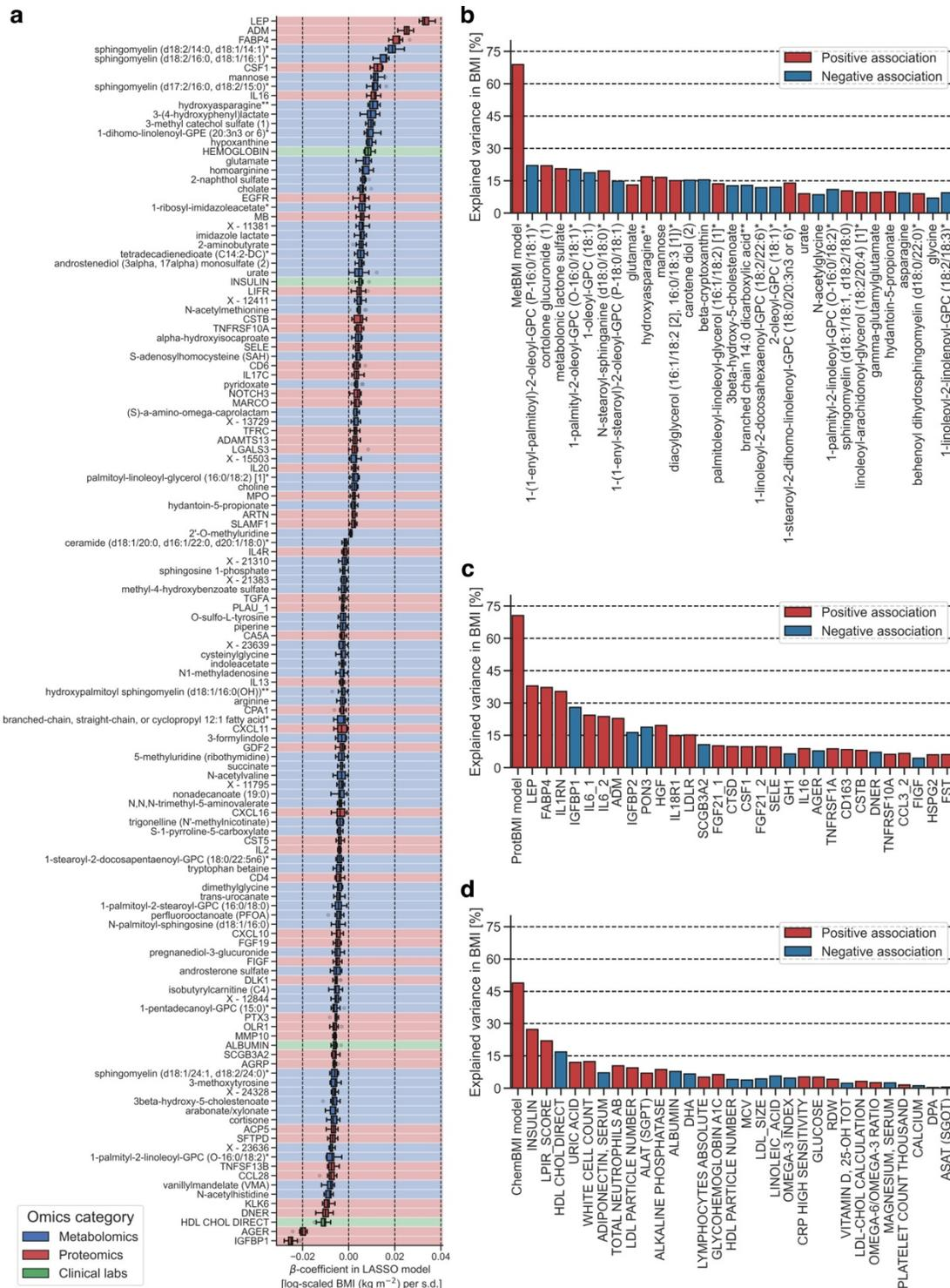


**Figure 2. Omics-based BMI estimates captured the variance in BMI better than any single analyte.**

**a** The variables that were retained across all ten combined omics-based Body Mass Index (CombiBMI) models (132 analytes: 77 metabolites, 51 proteins, and 4 clinical laboratory tests).  $\beta$ -coefficient was obtained from the fitted CombiBMI model with least absolute shrinkage and selection operator (LASSO) regression. Each background color corresponds to the analyte category. Data:

1116  
1117  
1118  
1119  
1120  
1121  
1122

1123 median (center line),  $[Q_1, Q_3]$  (box limits),  $[x_{\min}, x_{\max}]$  (whiskers), where  $Q_1$  and  $Q_3$  are the 1st and 3rd  
1124 quartile values, and  $x_{\min}$  and  $x_{\max}$  are the minimum and maximum values in  $[Q_1 - 1.5 \times \text{IQR}, Q_3 + 1.5$   
1125  $\times \text{IQR}]$  (IQR: the interquartile range,  $Q_3 - Q_1$ ), respectively;  $n = 10$  models. **b–d** Univariate explained  
1126 variance in BMI by each metabolite (**b**), protein (**c**), or clinical laboratory test (**d**). BMI was  
1127 independently regressed on each of the analytes that were retained in at least one of the ten LASSO  
1128 models (209 metabolites, 74 proteins, 41 clinical laboratory tests; Supplementary Data 5), using  
1129 ordinary least squares (OLS) linear regression with sex, age, and ancestry principal components (PCs)  
1130 as covariates. Multiple testing was adjusted with the Benjamini–Hochberg method across the 210 (**b**),  
1131 75 (**c**), or 42 (**d**) regressions, including each omics-based BMI (MetBMI: metabolomics-based BMI,  
1132 ProtBMI: proteomics-based BMI, ChemBMI: clinical chemistries-based BMI) model as reference.  
1133 Among the analytes that were significantly associated with BMI (180 metabolites, 63 proteins, 30  
1134 clinical laboratory tests), only the top 30 significant analytes are presented with their univariate  
1135 variances.  
1136

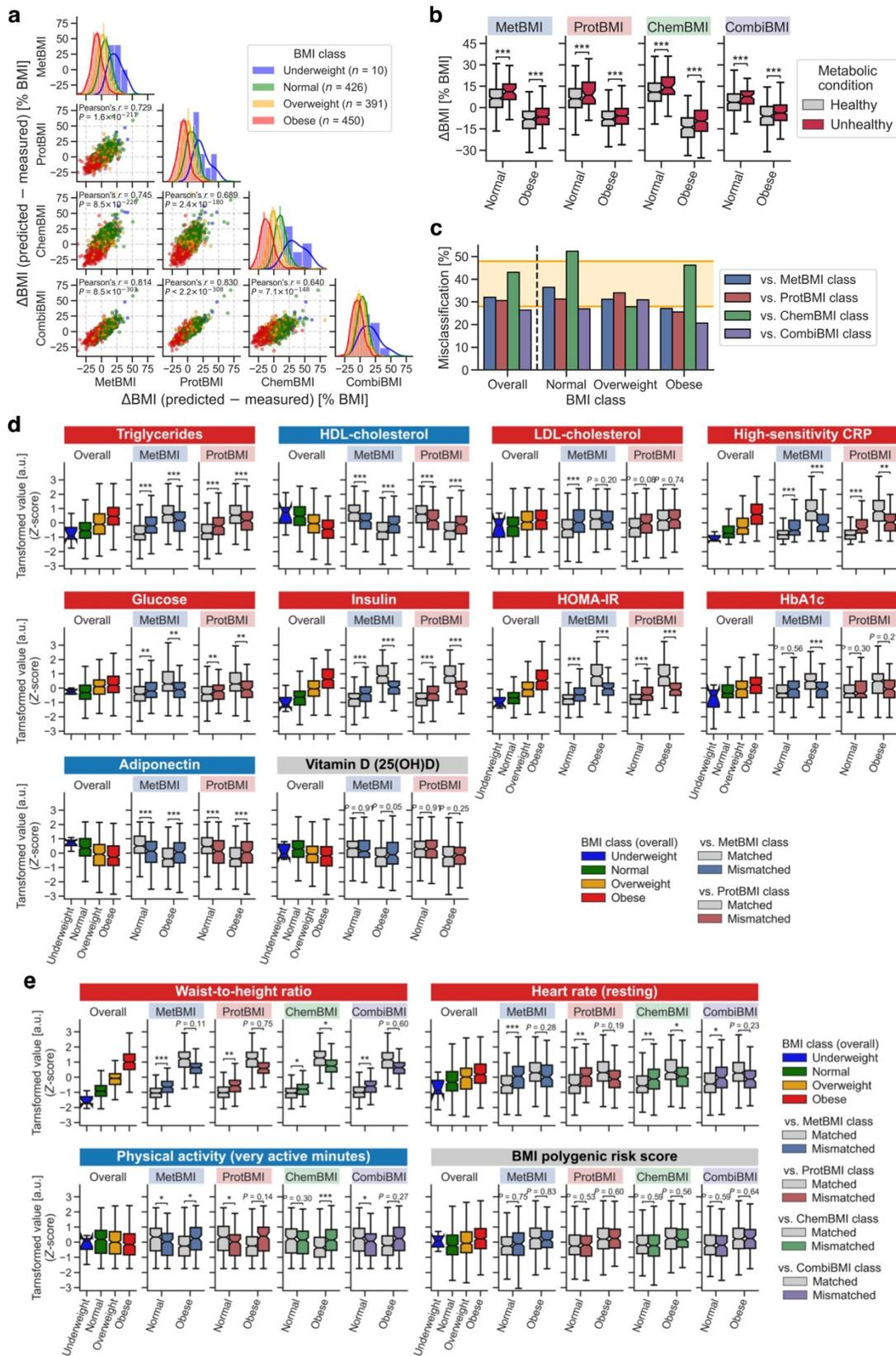


**Figure 3. Metabolic heterogeneity was responsible for the high rate of misclassification within the standard BMI classes.**

1137

1138

1139

1140 **a** Difference of the omics-inferred Body Mass Index (BMI) from the measured BMI ( $\Delta$ BMI).  
1141 MetBMI: metabolomics-inferred BMI, ProtBMI: proteomics-inferred BMI, ChemBMI: clinical  
1142 chemistries-inferred BMI, CombiBMI: combined omics-inferred BMI,  $P$ : adjusted  $P$ -value of two-  
1143 sided Pearson's correlation test with the Benjamini–Hochberg method across the six combinations,  $n$ :  
1144 the number of participants in each BMI class (total  $n = 1,277$  participants). The line in histogram panel  
1145 indicates the kernel density estimate. **b** Difference in  $\Delta$ BMI between clinically-defined metabolic  
1146 health conditions within the normal or obese BMI class. Significance was assessed using ordinary  
1147 least squares (OLS) linear regression with BMI, sex, age, and ancestry principal components (PCs) as  
1148 covariates, while adjusting multiple testing with the Benjamini–Hochberg method across the eight  
1149 (two BMI classes  $\times$  four omics categories) regressions. **c** Misclassification rate of overall cohort or  
1150 each BMI class against the omics-inferred BMI class. Range of the previously reported  
1151 misclassification rate<sup>36,37</sup> is highlighted with orange background. Note that the underweight BMI class  
1152 is not presented due to small sample size, but its misclassification rate was 80% against CombiBMI  
1153 class and 100% against the others. **d**, **e** Difference in the obesity-related clinical blood marker (**d**) or  
1154 BMI-associated physiological feature (**e**) between Matched and Mismatched groups within the normal  
1155 or obese BMI class. Significance was assessed using OLS linear regression with BMI, sex, age, and  
1156 ancestry PCs as covariates, while adjusting multiple testing with the Benjamini–Hochberg method  
1157 across the 40 (**d**, 2 BMI classes  $\times$  2 omics categories  $\times$  10 markers) or 216 (**e**, 2 BMI classes  $\times$  4 omics  
1158 categories  $\times$  27 features) regressions. Four of the 27 features that were significantly associated with  
1159 BMI (Fig. 1c) are representatively presented in **e**, and the other results are found in Supplementary  
1160 Data 6. HDL: high-density lipoprotein, LDL: low-density lipoprotein, CRP: C-reactive protein,  
1161 HOMA-IR: homeostatic model assessment for insulin resistance, HbA1c: glycated hemoglobin A1c,  
1162 25(OH)D: 25-hydroxyvitamin D. **b**, **d**, **e** Data: median (center line), 95% confidence interval (CI)  
1163 around median (notch),  $[Q_1, Q_3]$  (box limits),  $[x_{\min}, x_{\max}]$  (whiskers), where  $Q_1$  and  $Q_3$  are the 1st and  
1164 3rd quartile values, and  $x_{\min}$  and  $x_{\max}$  are the minimum and maximum values in  $[Q_1 - 1.5 \times \text{IQR}, Q_3 +$   
1165  $1.5 \times \text{IQR}]$  (IQR: the interquartile range,  $Q_3 - Q_1$ ), respectively;  $n = 373$  (**b**, Healthy in Normal), 49  
1166 (**b**, Unhealthy in Normal), 208 (**b**, Healthy in Obese), 241 (**b**, Unhealthy in Obese) participants (see  
1167 Supplementary Data 6 for each sample size in **d** and **e**). \*Adjusted  $P < 0.05$ , \*\*adjusted  $P < 0.01$ ,  
1168 \*\*\*adjusted  $P < 0.001$ .  
1169

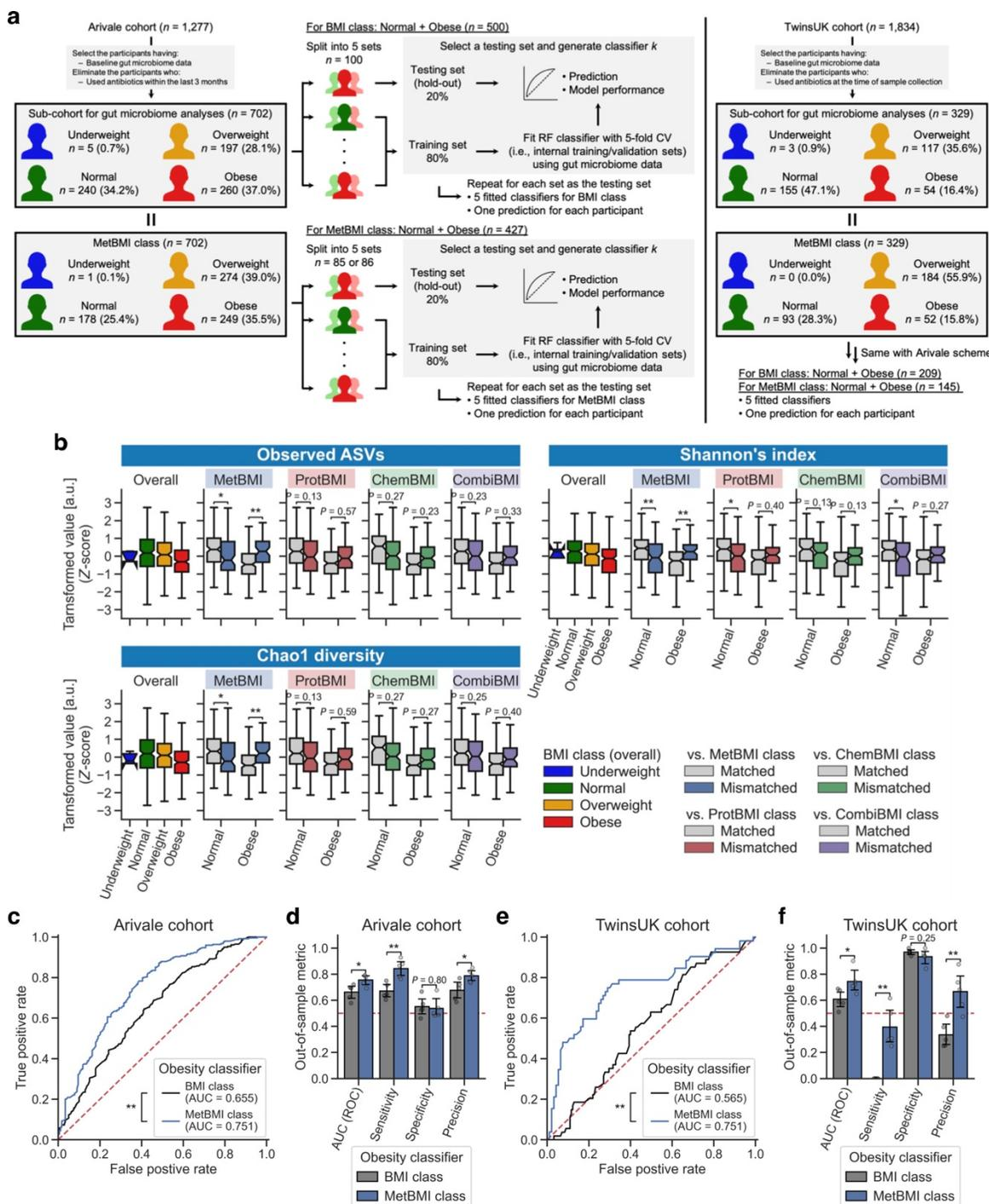


**Figure 4. Metabolomics-inferred BMI reflected gut microbiome profiles better than BMI.**

**a** Overview of study cohorts and the gut microbiome-based obesity classifier generation. BMI: Body Mass Index, MetBMI: metabolomics-inferred BMI, RF: random forest, CV: cross-validation. **b** Difference in gut microbiome  $\alpha$ -diversity between Matched and Mismatched groups within the normal or obese BMI class. Significance was assessed using ordinary least squares (OLS) linear regression with BMI, sex, age, and ancestry principal components (PCs) as covariates, while adjusting multiple testing with the Benjamini–Hochberg method across the 24 (2 BMI classes  $\times$  4 omics categories  $\times$  3 metrics) regressions. ProtBMI: proteomics-inferred BMI, ChemBMI: clinical chemistries-inferred

1170

1171

1172

1173

1174

1175

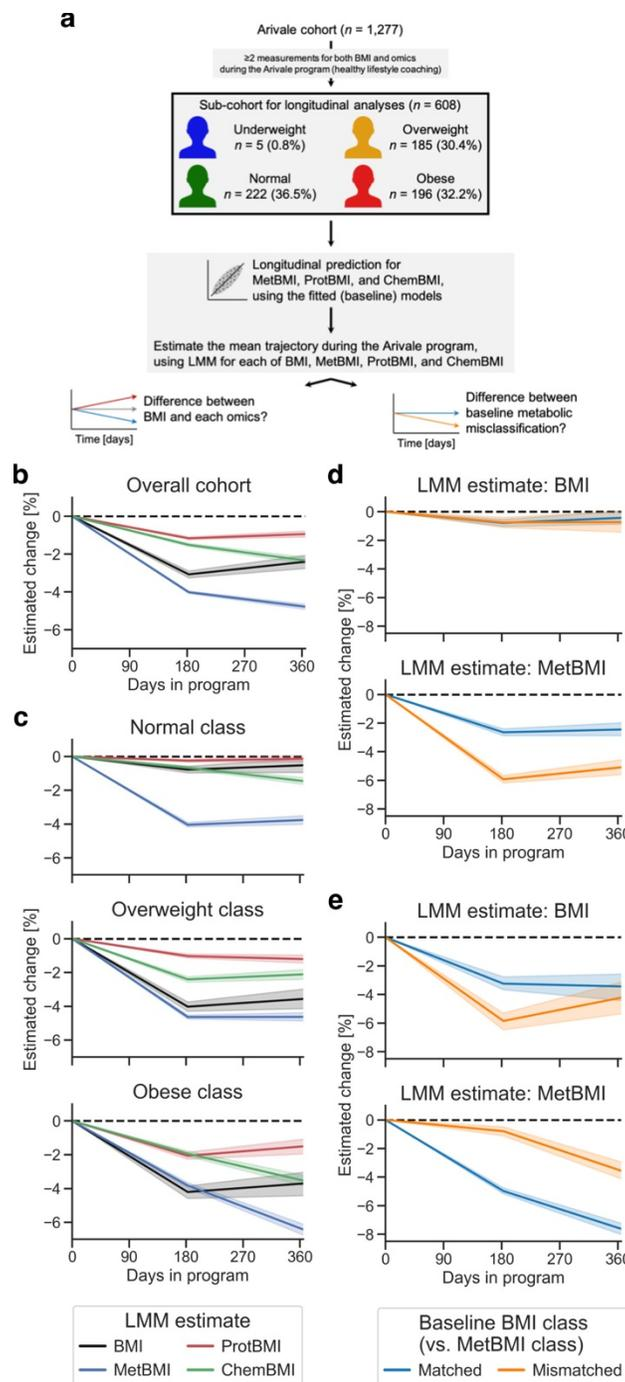
1176

1177

1178

1179 BMI, CombiBMI: combined omics-inferred BMI, ASV: amplicon sequence variant. Data: median  
1180 (center line), 95% confidence interval (CI) around median (notch),  $[Q_1, Q_3]$  (box limits),  $[x_{\min}, x_{\max}]$   
1181 (whiskers), where  $Q_1$  and  $Q_3$  are the 1st and 3rd quartile values, and  $x_{\min}$  and  $x_{\max}$  are the minimum  
1182 and maximum values in  $[Q_1 - 1.5 \times \text{IQR}, Q_3 + 1.5 \times \text{IQR}]$  (IQR: the interquartile range,  $Q_3 - Q_1$ ),  
1183 respectively.  $n = 240$  (Normal), 260 (Obese) participants (see Supplementary Data 6 for each sample  
1184 size). \*Adjusted  $P < 0.05$ , \*\*adjusted  $P < 0.01$ . **c, e** Receiver operator characteristic (ROC) curve of  
1185 the gut microbiome-based model classifying participants to the normal vs. obese class in the Arivale  
1186 (**c**) or TwinsUK (**e**) cohort. Each ROC curve was generated from the overall participants:  $n = 500$  (**c**,  
1187 BMI class), 427 (**c**, MetBMI class), 209 (**e**, BMI class), 145 (**e**, MetBMI class) participants. The red  
1188 dashed line indicates a random classification line. AUC: area under curve. \*\* $P < 0.01$  in two-sided  
1189 unpaired DeLong's test. **d, f** Comparison of model performance between the BMI and MetBMI  
1190 classifiers in the Arivale (**d**) or TwinsUK (**f**) cohort. Out-of-sample metric value was calculated from  
1191 each corresponding hold-out testing set. Data: mean with 95% CI,  $n = 5$  models. \* $P < 0.05$ , \*\* $P <$   
1192 0.01 in two-sided Welch's  $t$ -test.  
1193





1194

1195

1196

**Figure 5. Metabolic health of the metabolically obese group was substantially improved following a healthy lifestyle intervention.**

1197

1198

1199

1200

1201

1202

1203

**a** Overview of the longitudinal analysis using omics-inferred Body Mass Index (BMI). BMI: measured BMI, MetBMI: metabolomics-inferred BMI, ProtBMI: proteomics-inferred BMI, ChemBMI: clinical chemistries-inferred BMI, LMM: linear mixed model. **b, c** Longitudinal change in the omics-inferred BMI within the overall cohort (**b**) or within each baseline BMI class (**c**). Average trajectory of each measured or omics-inferred BMI was independently estimated using LMM with random effects for each participant (see Methods) in the overall cohort (**b**) or in each baseline BMI class-stratified group (**c**). **d, e** Longitudinal change in MetBMI of the misclassified participants within

1204 the normal (**d**) or obese (**e**) BMI class. Average trajectory of each BMI or MetBMI was independently  
1205 estimated using the above LMM with the baseline misclassification of BMI class against MetBMI  
1206 class as additional fixed effects (see Methods) in each baseline BMI class-stratified group. **b–e** The  
1207 dashed line corresponds to the baseline value of each estimate. Data: mean with 95% confidence  
1208 interval (CI);  $n = 608$  (**b**), 222 (**c**, Normal), 185 (**c**, Overweight), 196 (**c**, Obese), 137 (**d**, Matched), 85  
1209 (**d**, Mismatched), 139 (**e**, Matched), 57 (**e**, Mismatched) participants.  
1210

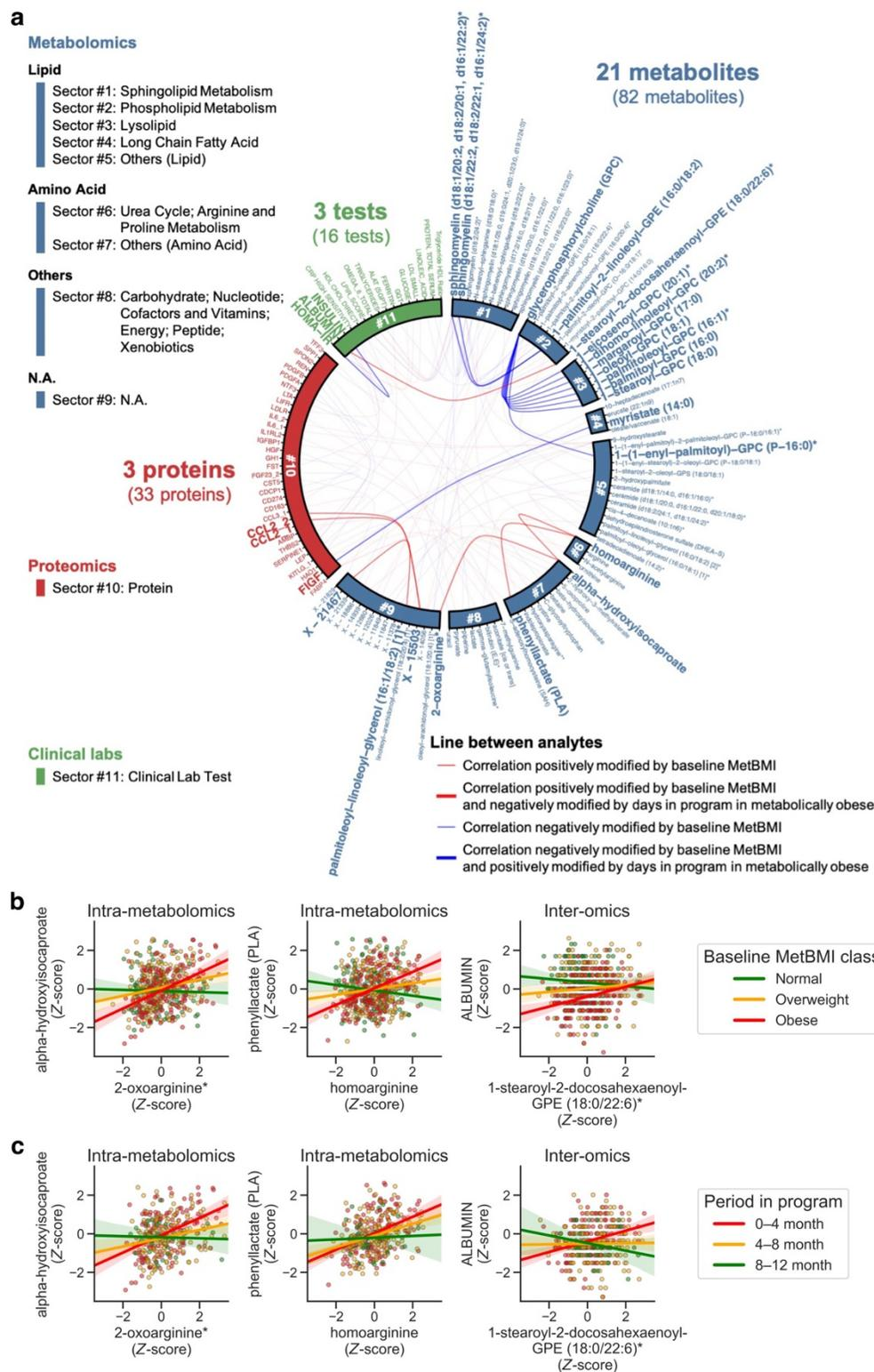


**Figure 6. Plasma analyte correlation network in the metabolically obese group shifted toward a structure observed in metabolically healthier state following a healthy lifestyle intervention.**

**a** Cross-omic interactions modified by metabolomics-inferred Body Mass Index (MetBMI) and days in the program. For each of the 608,856 pairwise relationships of plasma analytes (766 metabolites,

1211

1212

1213

1214

1215

1216 274 proteomics, 64 clinical laboratory tests), the baseline relationship between analyte–analyte pair  
1217 and MetBMI within the Arivale sub-cohort (Fig. 5a; 608 participants) was assessed using their  
1218 interaction term in each generalized linear model (GLM; see Methods), while adjusting multiple  
1219 testing with the Benjamini–Hochberg method. The 100 analyte–analyte pairs (82 metabolites, 33  
1220 proteins, 16 clinical laboratory tests; Supplementary Data 7) that were significantly modified by the  
1221 baseline MetBMI are presented. For each of these 100 pairs, the longitudinal relationship between  
1222 analyte–analyte pair and days in the program within the metabolically obese group (i.e., the baseline  
1223 obese MetBMI class; 182 participants) was further assessed using their interaction term in each  
1224 generalized estimating equation (GEE; see Methods), while adjusting multiple testing with the  
1225 Benjamini–Hochberg method. The 27 analyte–analyte pairs (21 metabolites, 3 proteins, 3 clinical  
1226 laboratory tests) that were significantly modified by days in the program are highlighted by line width  
1227 and label font size. **b, c** Representative examples of the analyte–analyte pair that was significantly  
1228 modified by both baseline MetBMI (**b**) and days in the program (**c**) in **a**. The solid line in each panel is  
1229 the ordinary least squares (OLS) linear regression line with 95% confidence interval (CI).  $n = 530$  (**b**,  
1230 left), 553 (**b**, center), 566 (**b**, right) participants;  $n = 324$  (**c**, left), 339 (**c**, center), 347 (**c**, right)  
1231 measurements from the 182 participants of the metabolically obese group. Of note, data points outside  
1232 of plot range are trimmed in these presentations.  
1233